An Evaluation of Advanced Dvorak Technique–Derived Tropical Cyclone Intensity Estimates during Extratropical Transition Using Synthetic Satellite Imagery

ALEXANDER MANION AND CLARK EVANS

Atmospheric Science Program, Department of Mathematical Sciences, University of Wisconsin–Milwaukee, Milwaukee, Wisconsin

TIMOTHY L. OLANDER AND CHRISTOPHER S. VELDEN

Cooperative Institute for Meteorological Satellite Studies, University of Wisconsin–Madison, Madison, Wisconsin

LEWIS D. GRASSO

Cooperative Institute for Research in the Atmosphere, Colorado State University, Fort Collins, Colorado

(Manuscript received 27 January 2015, in final form 8 May 2015)

ABSTRACT

It is known that both Dvorak technique and advanced Dvorak technique–derived intensity estimates for tropical cyclones during extratropical transition are less reliable because the empirical relationships between cloud patterns and cyclone intensity underlying each technique are primarily tropical in nature and thus less robust during extratropical transition. However, as direct observations of cyclone intensity during extratropical transition are rare, the precise extent to which such remotely sensed intensity estimates are in error is uncertain. To address this uncertainty and provide insight into how advanced Dvorak technique–derived intensity estimates during extratropical transition may be improved, the advanced Dvorak technique is applied to synthetic satellite imagery derived from 25 numerical simulations of Atlantic basin tropical cyclones—five cases, five microphysical parameterizations—during extratropical transition. From this, an internally consistent evaluation between model-derived and advanced Dvorak technique–derived cyclone intensity estimates is conducted. Intensity estimate error and bias peak at the beginning of extratropical transition and decline thereafter for maximum sustained surface wind. On average, synthetic advanced Dvorak technique–derived estimates of maximum sustained surface wind asymptote toward or remain near their weakest-possible values after extratropical transition begins. Minimum sea level pressure estimates exhibit minimal bias, although this result is sensitive to microphysical parameterization. Such sensitivity to microphysical parameterization, particularly with respect to cloud radiative properties, suggests that only qualitative insight regarding advanced Dvorak technique–derived intensity estimate error during extratropical transition may be obtained utilizing synthetic satellite imagery. Implications toward developing improved intensity estimates during extratropical transition are discussed.

1. Introduction

The current intensity of tropical cyclones (TCs) can be assessed using either direct observations or remotely sensed estimates from meteorological satellites. However, direct observations of TC intensity, such as by reconnaissance aircraft, buoys, ships, oil rigs, and land-based observation stations, are relatively sparse. Consequently, satellite estimates are chiefly relied upon to assess the intensity of the vast majority of TCs, particularly outside of the North Atlantic basin (e.g., Velden et al. 2006). This is primarily accomplished utilizing the Dvorak technique (DT; Dvorak 1984), an internally consistent, empirical method that an analyst uses to relate organized TC cloud patterns to cyclone intensity. Further information regarding the DT is provided by Dvorak (1984) and Velden et al. (2006). Brown and Franklin

Corresponding author address: Dr. Clark Evans, Atmospheric Science Program, Dept. of Mathematical Sciences, University of Wisconsin–Milwaukee, P.O. Box 413, Milwaukee, WI 53201.
E-mail: evans36@uwm.edu

DOI: 10.1175/WAF-D-15-0019.1

(2004) found that approximately 50% of DT-based Atlantic TC intensity estimates are within 5 knots (kt; for maximum sustained surface wind; $1\,\text{kt} = 0.51\,\text{m}\,\text{s}^{-1}$) of reconnaissance aircraft–aided best-track intensity estimates.

Despite the enduring success of the DT, it is not without its limitations. One primary limitation of the DT lies in its inherent subjectivity owing to the varying expertise levels of analysts who use it to obtain TC intensity estimates (Velden et al. 2006). The advanced Dvorak technique (ADT; Olander and Velden 2007), a fully automated, objective means of assessing TC intensity from satellite imagery, was originally developed out of a desire to mitigate the subjective nature of the DT. The mature ADT algorithm has evolved and is not just an objective application of the DT; rather, through modifications based upon rigorous statistical and empirical analysis, the ADT extends and, in some cases, improves upon the original DT. ADT performance is competitive with a consensus of all available subjective operational DT intensity estimates with both sources of estimates exhibiting an overall small weak-intensity bias (Olander and Velden 2007). Further information regarding the ADT is provided by Olander and Velden (2007, 2013).

Both DT- and ADT-derived TC intensity estimates are less reliable during extratropical transition (ET; Jones et al. 2003), or the process by which a TC transforms into an extratropical cyclone (Velden et al. 2006). As a TC undergoes ET, the development of the prototypical conveyor belt features associated with extratropical cyclones (e.g., Carlson 1980; Browning 1990) results in deep, moist convection becoming increasingly asymmetric about the TC's center. Descent associated with the cyclone's developing dry intrusion results in the erosion of deep, moist convection near and equatorward of the TC's center. Concurrently, ascent associated with the cyclone's developing warm conveyor belt results in the formation of a delta-shaped expanse of shallow to moderately deep moist convection poleward and eastward of the TC (Klein et al. 2000). The resultant cloud pattern most closely resembles the shear or, less commonly, curved band "scene types" [e.g., section 5.B of Olander and Velden (2013)] as identified by both the DT and ADT. These scene types are those typically associated with the weakest DT- and ADT-derived intensity estimates (Dvorak 1984; Olander and Velden 2013).

Consequently, the loss of deep, moist convection near the center of the transitioning TC and the increasing distance from the center to which the remaining convection becomes displaced results in DT- (and ADT-) derived intensity estimates that are unrepresentative (Miller and Lander 1997). In other words, TC intensity typically does not decay during ET as rapidly as DT- and/or ADT-derived intensity estimates would suggest, even when the decay of such intensity estimates is constrained [e.g., rule 9 of Dvorak (1984); the ADT weakening flag of Olander and Velden (2013)]. This occurs as the transitioning TC begins to extract kinetic energy from the available potential energy associated with the vertically sheared background flow, which enables the TC to maintain its intensity during ET to a greater extent than if it primarily drew energy from the underlying ocean surface (and its ultimate vertical transport by and release in regions of active deep, moist convection). Further, the cyclone's pressure–wind relationship changes as its wind field expands (Evans and Hart 2008), such that the tropical, basin-specific pressure–wind relationships used by the DT and ADT no longer necessarily hold. Summarizing, DT- and ADT-derived TC intensity estimates during the ET process become less reliable because the empirical relationships between the associated cloud patterns and storm intensity that underlie each technique were primarily derived during tropical stages and are therefore less robust during and after ET.

The specific extent of the degradation in reliability in DT- and ADT-derived intensity estimates during ET has been difficult to document, primarily because of the lack of verifying observations. Miller and Lander (1997) note that DT-derived intensity estimates for "a significant number" of recurving TCs during the 1994 and 1995 western North Pacific TC seasons were weak biased, in some cases by as much as three Dvorak "*T*" numbers. With respect to the ADT, we conduct a limited verification of ADT-derived intensity estimates for TCs within the preceding two days of completing ET, given by the time that a given TC is classified as extratropical within the National Hurricane Center "best track" database (Jarvinen et al. 1984), in the North Atlantic basin between 2005 and 2008. The storms forming this composite are Cindy, Katrina, Ophelia, and Wilma from 2005; Alberto, Beryl, and Ernesto from 2006; Barry and Noel from 2007; and Hanna, Ike, and Kyle from 2008. While many of these storms made landfall, only pre- or at-landfall intensities were evaluated against validation data obtained from in situ reconnaissance aircraft or landfall intensity measurements. In the composite mean ($n = 18$), final ADT current intensity estimates for maximum sustained 10-m wind speed $v_{\max}$ during ET exhibit a 13.12-kt weak bias with a root-mean-square error of 14.26 kt. For reference, these values are larger than those typically found with the ADT (Olander and Velden 2007) and DT (Brown and Franklin 2004) and are comparable to the uncertainty in satellite-derived best-track estimates in the North Atlantic basin (Landsea and Franklin 2013).

The majority of the cases noted above occur early in the ET process and are not found at higher latitudes near the completion of ET. Direct observations of v_{max} and minimum sea level pressure p_{min} during ET are virtually nonexistent. Routine reconnaissance aircraft missions, conducted primarily in the North Atlantic basin, typically cease as a targeted TC enters the midlatitudes if it poses no threat to land. Furthermore, there are relatively few permanent (buoys, oil rigs) or transient (ships) observing platforms along the primary midlatitude oceanic storm tracks. Thus, while DT- and ADT-derived intensity estimates are known to be less reliable and thought to be weak biased during at least some ET events, the precise magnitudes and temporal behavior (e.g., from ET start through its completion) of such errors and bias are unknown as a result of a lack of observations against which DT- and ADT-derived intensity estimates may be verified.

An alternative satellite-based technique for assessing the current intensity of TCs during ET was proposed by Miller and Lander (1997). Their technique, dubbed the XT method, resembles a modified form of the procedure used to estimate TC intensity for the DT "curved band" cloud pattern type. Intensity estimates are made in consideration of 1) the arc length of the TC's primary outer cloud band that is not connected to its center; 2) the organizational extent of the TC's lower tropospheric circulation, assessed from the organization and extent of shallow convection westward and equatorward of the TC's center; 3) the existence of deep, moist convection near the TC's center; and 4) the TC's forward motion. Greater arc length, a better-organized circulation, the presence of inner-core deep, moist convection, and a faster translational speed are each associated with more intense XT intensity estimates. It should be noted that similar considerations enter into the Hebert–Poteat method for estimating the intensity of subtropical cyclones (Hebert and Poteat 1975). The XT method has been used operationally by the Joint Typhoon Warning Center since the 1997 North Pacific typhoon season (e.g., Dillon and Andrews 1998) and by the National Hurricane Center in deriving best-track intensity estimates for an unnamed subtropical storm in 2000 (Beven 2000). However, no documented verification of this method exists.

Herein, we explore whether synthetic satellite imagery [e.g., Bikos et al. (2012) and references therein], as derived utilizing a forward radiative transfer model applied to numerical model simulation output, can be used to evaluate ADT performance during ET. Synthetic satellite imagery provides an accessible yet effective means of visualizing numerical model simulations (Bikos et al. 2012). Its utility is contingent upon the numerical model's ability to accurately simulate cloud morphology and the evolution of the atmospheric state (Otkin et al. 2009). With respect to the former, there is much sensitivity to microphysical parameterization and its handling of upper-tropospheric hydrometeor species, particularly cloud ice (e.g., Otkin and Greenwald 2008; Otkin et al. 2009; Jankov et al. 2011; Bikos et al. 2012; Van Weverberg et al. 2013; Jin et al. 2014; Cintineo et al. 2014; Grasso et al. 2014). Consequently, it is unknown whether synthetic satellite imagery can effectively be utilized by the ADT to infer scene type and cyclone intensity from raw values of and spatial gradients in longwave infrared brightness temperature.

The research presented herein thus attempts to address the following two questions:

1) Can reliable ADT-derived intensity estimates for numerically simulated TCs be obtained utilizing synthetic satellite imagery produced from numerical simulation output?
2) If so, through an internally consistent comparison of model-derived v_{max} and p_{min} to ADT-derived (from synthetic satellite imagery) v_{max} and p_{min}, what is the nature of the ADT-derived TC intensity estimate error and bias during ET?

Alternatively, the first of these questions may be posed as: Do the relationships between TC cloud patterns and TC intensity that serve as the underpinnings for the ADT hold for numerically simulated TCs, particularly in light of sensitivity in the former to cloud microphysics parameterization? The remainder of this manuscript is structured as follows. Study methodology, including numerical simulation formulation, case selection, the derivation of synthetic satellite imagery, and the application of the ADT to simulation output, is described in section 2. Key findings from this research are presented in section 3. A discussion of how these key findings motivate future research toward improved TC intensity estimates during ET is presented alongside a summary of the work in section 4.

2. Methodology

a. Numerical simulations

Numerical simulations are conducted utilizing the Advanced Research version of the Weather Research and Forecasting Model, version 3.4.1 (ARW; Skamarock et al. 2008). A horizontal grid spacing of 4 km over a single 4000 km × 4000 km domain centered at 37°N, 63.5°W with 30 terrain-following hybrid sigma vertical levels is used for all simulations. Davis et al. (2008) demonstrated that horizontal grid spacing of

4 km allows for somewhat realistic explicit simulated representations of the tropical cyclone inner core and rainbands, although objective verification of such features against inner-core observations remains elusive. Spacing between individual vertical levels is approximately 20–40 hPa in the lower troposphere, 60–80 hPa in the midtroposphere, and 30–40 hPa near the tropopause. Simulation length for all cases is 120 h. Initial and lateral boundary conditions for each simulation are provided by the ECMWF's ERA-Interim with horizontal grid spacing of approximately 0.7° latitude and longitude and 6-hourly temporal frequency (Dee et al. 2011). No TC bogus or assimilation of operational TC information is applied to artificially improve upon the initial representation of each TC. All simulations utilize the Yonsei University planetary boundary layer (Hong et al. 2006), RRTM for Global Climate Models (RRTMG) shortwave and longwave radiation (Iacono et al. 2008), revised MM5 similarity surface layer [Jimenez et al. (2012), their section 2a], and unified Noah land surface (Chen and Dudhia 2001) parameterizations. Deep, moist convection is treated explicitly, or without parameterization. The Garratt (1992) formulation for the enthalpy transfer coefficient is utilized as it is believed to be most appropriate for TC simulations.

Given the previously mentioned sensitivity of synthetic satellite imagery to the choice of microphysical parameterization, five simulations—each utilizing a different microphysical parameterization—are conducted for each of the five cases (section 2b) considered herein. Thus, a total of 25 numerical simulations are conducted. The five selected parameterizations utilized are the WSM6 (Hong and Lim 2006), Thompson (Thompson et al. 2008), Morrison (Morrison et al. 2009), Milbrandt–Yau (Milbrandt and Yau 2005), and WRF double-moment 6-class (WDM6; Lim and Hong 2010) parameterizations. Each predicts the mixing ratio for water vapor and five microphysical hydrometeor species: rainwater, cloud water, snow, cloud ice, and graupel and/or hail. The Milbrandt–Yau parameterization also predicts the number concentration for all microphysical species and maintains separate classes for graupel and hail. The Morrison parameterization predicts number concentrations for all species except cloud water, the Thompson parameterization predicts number concentrations only for cloud ice and rainwater, and the WDM6 parameterization predicts number concentrations for rainwater, cloud water, and cloud condensation nuclei. A succinct summary of the fundamental differences between the WSM6, Thompson, and Morrison parameterizations is provided by Van Weverberg et al. (2013).

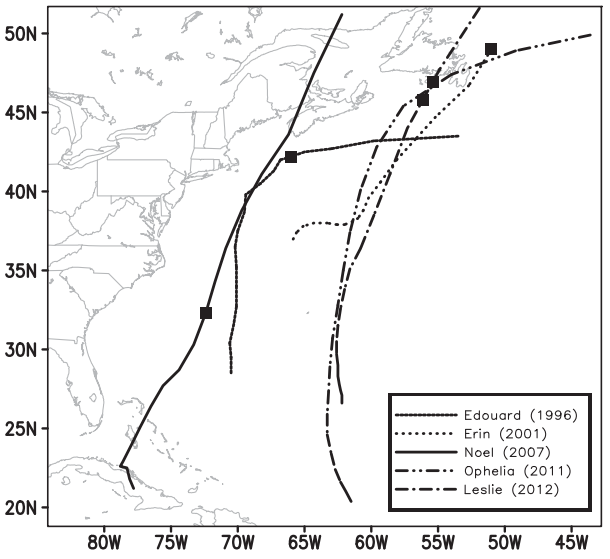

FIG. 1. Model simulation domain with the National Hurricane Center best-track positions, at 6-hourly intervals, for each of the five TCs examined within this work. Only the track of each TC during the time period over which it is simulated within the domain is depicted. The filled black squares along each track denote the location at which the National Hurricane Center declared the TC to have completed ET.

b. *Case selection*

Simulations are conducted for five selected cases, each representing an observed ET event in the North Atlantic basin between 1996 and 2012: Edouard (1996; Pasch and Avila 1999), Erin (2001; Beven et al. 2003), Noel (2007; Brennan et al. 2009), Ophelia (2011; Avila and Stewart 2013), and Leslie (2012; Stewart 2013). Each TC completed ET, as assessed utilizing National Hurricane Center best-track data, and remained over open water during ET. The observed tracks of each TC are overlain with the simulation domain in Fig. 1. Simulations of each case begin approximately 48–72 h prior to the start of ET so as to allow sufficient time for the simulated vortex and its microphysical fields to spin up prior to the start of our analysis (described in section 2d below). Simulations of Edouard, Erin, Noel, Ophelia, and Leslie end 36, 24, 24, 26, and 21 h after the end of ET, respectively, as assessed utilizing National Hurricane Center best-track data. The selected cases reflect a variety of ET evolutions [e.g., time to complete ET, intensity at the start and end of ET, and thermal structure evolution; Hart et al. (2006)], as determined utilizing National Hurricane Center best-track data and cyclone phase-space (Hart 2003) trajectory plots for each case derived from 6-h ERA-Interim data. These attributes are summarized in Table 1.

c. *Synthetic satellite imagery*

Synthetic satellite imagery is created using the Community Radiative Transfer Model, version 2.0.5 (CRTM;

TABLE 1. Intensity, thermal structure, and timing information during ET for each of the five cases considered herein. The time at which ET began (ET start time) and the posttransition thermal structure for each case are derived following Evans and Hart (2003) as applied to ERA-Interim data. The time at which ET completed (ET end time) and all intensity information (p_{min}, v_{max}) for each case are obtained from the National Hurricane Center best-track database.

Case	Simulation start time	ET start time	ET end time	Post-ET thermal structure	ET start intensity	ET end intensity
Edouard (1996)	1800 UTC 30 Aug	0000 UTC 2 Sep	0600 UTC 3 Sep	Cold core	964 hPa, 80 kt	985 hPa, 55 kt
Erin (2001)	0600 UTC 11 Sep	1800 UTC 13 Sep	0600 UTC 15 Sep	Cold core	982 hPa, 70 kt	981 hPa, 60 kt
Noel (2007)	0000 UTC 31 Oct	0600 UTC 2 Nov	0000 UTC 3 Nov	Warm seclusion	981 hPa, 70 kt	980 hPa, 70 kt
Ophelia (2011)	1200 UTC 29 Sep	0600 UTC 2 Oct	1000 UTC 3 Oct	Cold core	945 hPa, 110 kt	990 hPa, 60 kt
Leslie (2012)	0600 UTC 7 Sep	1200 UTC 10 Sep	0900 UTC 11 Sep	Cold core	980 hPa, 65 kt	968 hPa, 65 kt

Han et al. 2006). Synthetic GOES-East 10.7-μm imagery is produced for each of the numerical simulations described above. Gaseous optical depths, which are a function of wavelength and sensor, are obtained from simulated three-dimensional fields of pressure (hPa), temperature (K), and water vapor mixing ratio (g kg^{-1}). Canopy temperatures (K) and monthly averaged, spectrally dependent, surface emissivity values (Seemann et al. 2008) are used as lower boundary conditions for the CRTM. The particle radius (μm) of each microphysical habit type (cloud, rain, snow, graupel, and ice) is precomputed and is subsequently passed into the CRTM. Such formulations take advantage of an assumed particle shape and size distribution along with values of the mass mixing ratio (g kg^{-1}) and, when predicted, number concentrations (kg^{-1}). Information regarding the specific particle size distributions utilized by the WSM6, Thompson, Morrison, Milbrandt–Yau, and WDM6 microphysical parameterizations may be found in Hong and Lim (2006), Thompson et al. (2008), Morrison et al. (2009), Milbrandt and Yau (2005), and Lim and Hong (2010), respectively. Top-of-the-atmosphere radiance values from the CRTM are then converted into synthetic GOES-East 10.7-μm brightness temperatures at an hourly interval from each simulation.

d. ADT application and evaluation

In this study, the performance of the ADT during ET is evaluated utilizing an internally consistent comparison between model-derived hourly time series of v_{max} and p_{min} (hereafter truth) and hourly time series of v_{max} and p_{min} derived from applying ADT, version 8.1.5, to synthetic satellite imagery obtained from each model simulation (hereafter synthetic ADT). In this version of ADT, p_{min} is obtained by utilizing the pressure–wind relationship of Knaff and Zehr (2007) and Courtney and Knaff (2009), wherein model-derived values of cyclone latitude, translation speed, mean radius of 34-kt (gale force) 10-m wind, and sea level pressure of the outermost closed isobar are utilized in conjunction with the synthetic ADT-derived value of v_{max} to obtain p_{min}. Error statistics—herein root-mean-square error (RMSE) and bias—are computed utilizing "synthetic ADT" minus "model." Thus, positive (negative) values of this difference for v_{max} (p_{min}) denote that the synthetic ADT-estimated intensity is too high compared to model truth. Evaluation of synthetic ADT performance begins 18 h into each model simulation so as to allow sufficient time for the simulated microphysical species (i.e., cloud fields) to spin up. The National Hurricane Center best-track intensity for each TC is used as the first-guess ADT intensity at t = 18 h. Synthetic ADT-derived intensity estimates during ET, typically occurring between 48 and 96 h into each simulation, are insensitive to whether the best-track or model-derived intensity is used as the first-guess ADT intensity at t = 18 h (not shown). This occurs as ADT's "memory" of previous intensity estimates, as manifest by the Dvorak (1984) weakening flag (rule 9) and constraint limits (rule 8), is limited to approximately 24 h (Olander and Velden 2013).

First-guess TC center positions at all times are provided by the location of the simulated 850-hPa geopotential height minimum. The spiral-centering/ring-fitting autocentering technique described by Olander and Velden (2007) is applied to update these positions if the synthetic ADT current intensity (CI No.) at the previous time (t − 1 h) is greater than 3.5. To facilitate comparison of results between cases, all error statistics are presented with respect to the ET timeline of Hart et al. (2006). Particular emphasis is given to the milestones of 24 h prior to ET start (T_B − 24 h), ET start (T_B; development of substantial cross-cyclone thermal asymmetry), the midpoint of ET (T_{MID}), and ET end (T_E; loss of warm-core thermal structure), each as determined utilizing the cyclone phase space of Hart (2003). Please note that the T_B utilized herein does not refer to brightness temperature, which is often referred to as T_b. To ensure that the evaluated intensity estimates are representative, hourly model truth and synthetic ADT-derived values of both v_{max} and p_{min} are averaged

over a ±1-h interval centered on the ET milestones for each simulation. The results are insensitive to the specific interval (±1 vs ±3 h or no averaging) over which these values are averaged (not shown).

Note that the evaluation conducted herein is between two model-derived quantities and not between model-derived and observed quantities. While the model simulations faithfully replicate the observed track and the transition from a tropical to an extratropical cyclone for most cases, it is impossible to assess whether each simulation faithfully replicates the actual intensity for each TC in the absence of direct intensity observations during ET. Model deviations from the best-track and/or actual intensity for each TC do exist for both $p_{\min}$ (Fig. 2) and $v_{\max}$ (Fig. 3). Potential causes of such departures include sensitivity to microphysical parameterization (e.g., Zhu and Zhang 2006; Jin et al. 2014), particularly for the Thompson- and Morrison-based simulations of Ophelia (2011); the initialization of each simulation with a coarse reanalysis TC vortex, particularly for Edouard (1996) and Erin (2001), the two strongest TCs at simulation start time; and insufficient treatment of TC-induced upwelling within the reanalysis-derived representation of the oceanic state for Leslie (2012; see also Stewart 2013).

These factors motivate the choice of the internally consistent, model-focused approach utilized herein. Consequently, our selection of five observed North Atlantic ET events to simulate rather than, for instance, idealized ET cases, is motivated primarily by a desire to examine the ADT's performance with physically realistic events reflecting a variety of TC evolutions during ET. It should be noted, however, that this methodology implicitly requires that the numerical model is capable of accurately simulating the relationship between the mass (e.g., pressure) and kinematic (e.g., wind) fields before, during, and after ET.

3. Results

a. Overall ADT error and bias during ET

The composite mean RMSEs for $v_{\max}$ and $p_{\min}$ during ET, each comprised of data from 23 numerical simulations, are depicted by the solid gray lines in Figs. 4a and 4c, respectively. Note that the composite mean does not include the Thompson- and Morrison-based simulations of Ophelia (2011) as the simulated TC was unable to complete ET in the strongly sheared environment in which it was embedded. The composite mean RMSE for $v_{\max}$ (Fig. 4a) increases between $T_B - 24$ h and T_B and decreases thereafter, whereas the composite mean RMSE for $p_{\min}$ decreases throughout ET. Utilizing a two-tailed Student's t test applied to the approximately normally distributed data, all changes in composite mean RMSE for $v_{\max}$ between successive milestones are statistically significant to ≥90% confidence. However, none of the changes in composite mean RMSE between successive milestones for $p_{\min}$ are statistically significant to ≥90% confidence.

The composite mean bias for $v_{\max}$ and $p_{\min}$ during ET, each again composed of data from 23 numerical simulations, are depicted by the solid gray lines in Figs. 5a and 5c, respectively. For $v_{\max}$, composite mean synthetic ADT-derived intensity estimates exhibit a large weak bias of approximately 20 kt at all times. As with RMSE, the composite mean bias for $v_{\max}$ increases between $T_B - 24$ h and T_B and decreases thereafter. However, the decrease in composite mean bias for $v_{\max}$ after T_B is not statistically significant to ≥90% confidence. For $p_{\min}$, composite mean synthetic ADT-derived intensity estimates are slightly strong biased at $T_B - 24$ h and slightly weak biased thereafter. The change in the sign of the bias that occurs between $T_B - 24$ h and T_B is statistically significant to ≥99% confidence; however, changes in the magnitude of the weak bias that occur after T_B are not statistically significant to ≥90% confidence. As before, all statistical significance testing is done utilizing a two-tailed Student's t test applied to the approximately normally distributed data.

During ET, synthetic ADT-derived intensity estimates for $v_{\max}$ (Fig. 6) become weaker or, in some cases, remain weak (e.g., $v_{\max} \leq 35$ kt). This occurs as strong vertical wind shear causes deep, moist convection to gradually become less well organized, as inferred by the evolution of the ADT-derived scene type (Fig. 7), and displaced increasingly farther from the center of the transitioning TC (e.g., Figs. 8b,d,f,h,j). This results in synthetic ADT-derived intensity estimates for $v_{\max}$ rapidly decaying to or remaining near their minimum-possible values early during ET. While $v_{\max}$ typically weakens during ET in both the model simulations (Fig. 3) and their observed counterparts (Table 1), it does not do so as rapidly as do synthetic ADT-derived values of $v_{\max}$ (Fig. 6). Consequently, the ADT-derived intensity RMSE and bias (Figs. 4a and 5a) peak in magnitude at T_B, when the discrepancy between the model-simulated and synthetic ADT-derived values of $v_{\max}$ is largest, and decline slightly thereafter as the model-simulated $v_{\max}$ becomes weaker.

As deep, moist convection weakens and is displaced to increasingly large radii during ET (Figs. 8 and 10–13), synthetic ADT-derived estimates of $p_{\min}$ (Fig. 9) converge toward a common value for each set of simulations of a given TC. This results from the use of the current ADT pressure–wind relationship, which utilizes

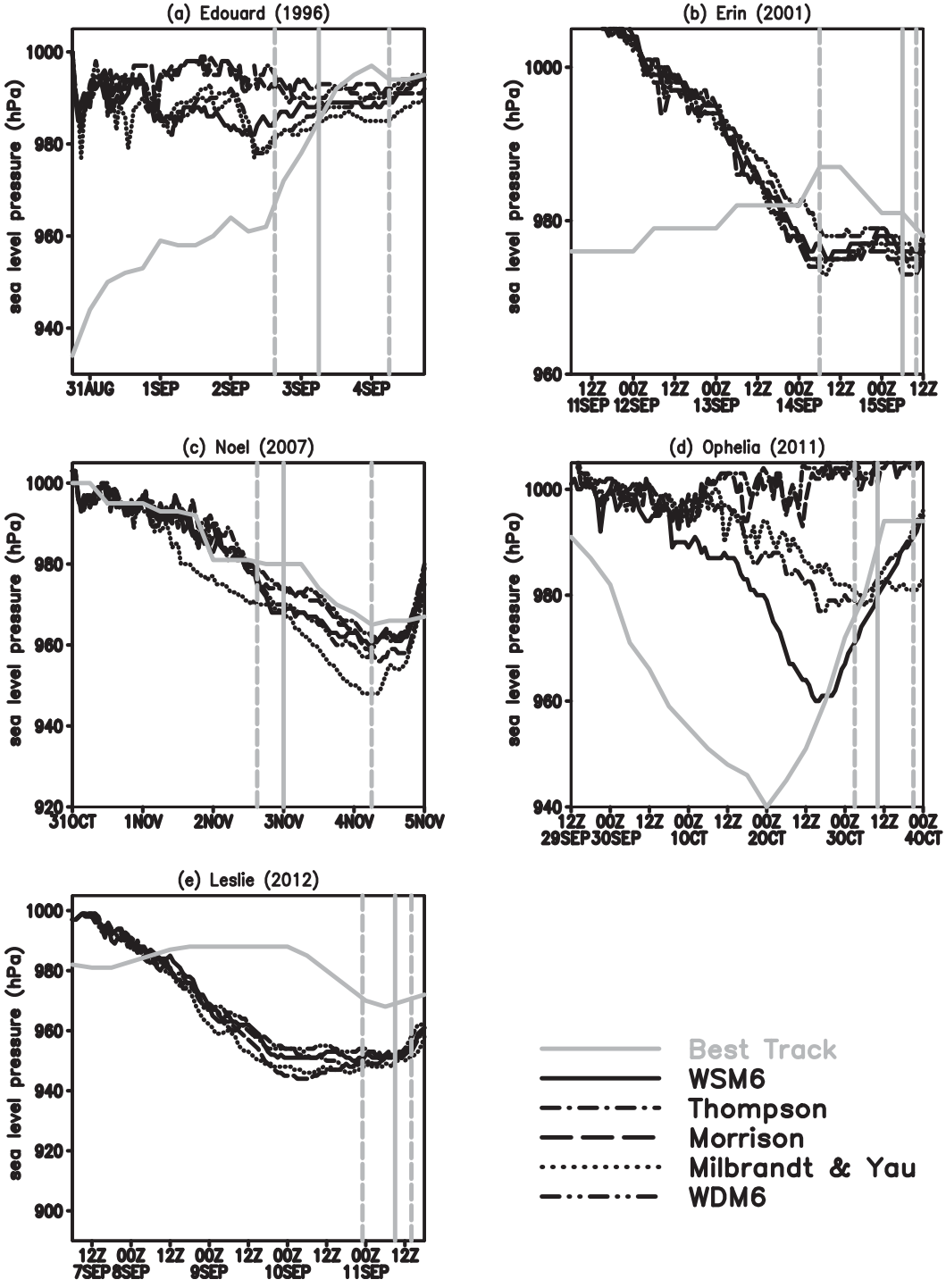

FIG. 2. Minimum sea level pressure $p_{\min}$ (hPa) from the National Hurricane Center best-track (solid gray) and the WSM6- (solid black), Thompson- (dash–dot), Morrison- (long dash), Milbrandt–Yau- (dot), and WDM6- (dash–dot–dot) based simulations for (a) Edouard (1996), (b) Erin (2001), (c) Noel (2007), (d) Ophelia (2011), and (e) Leslie (2012). The temporal axis in each panel begins 12 h into each model simulation. The left and right vertical gray dashed lines in each panel reflect the model consensus T_B and T_E, while the vertical gray solid line in each panel reflects the National Hurricane Center–designated T_E.

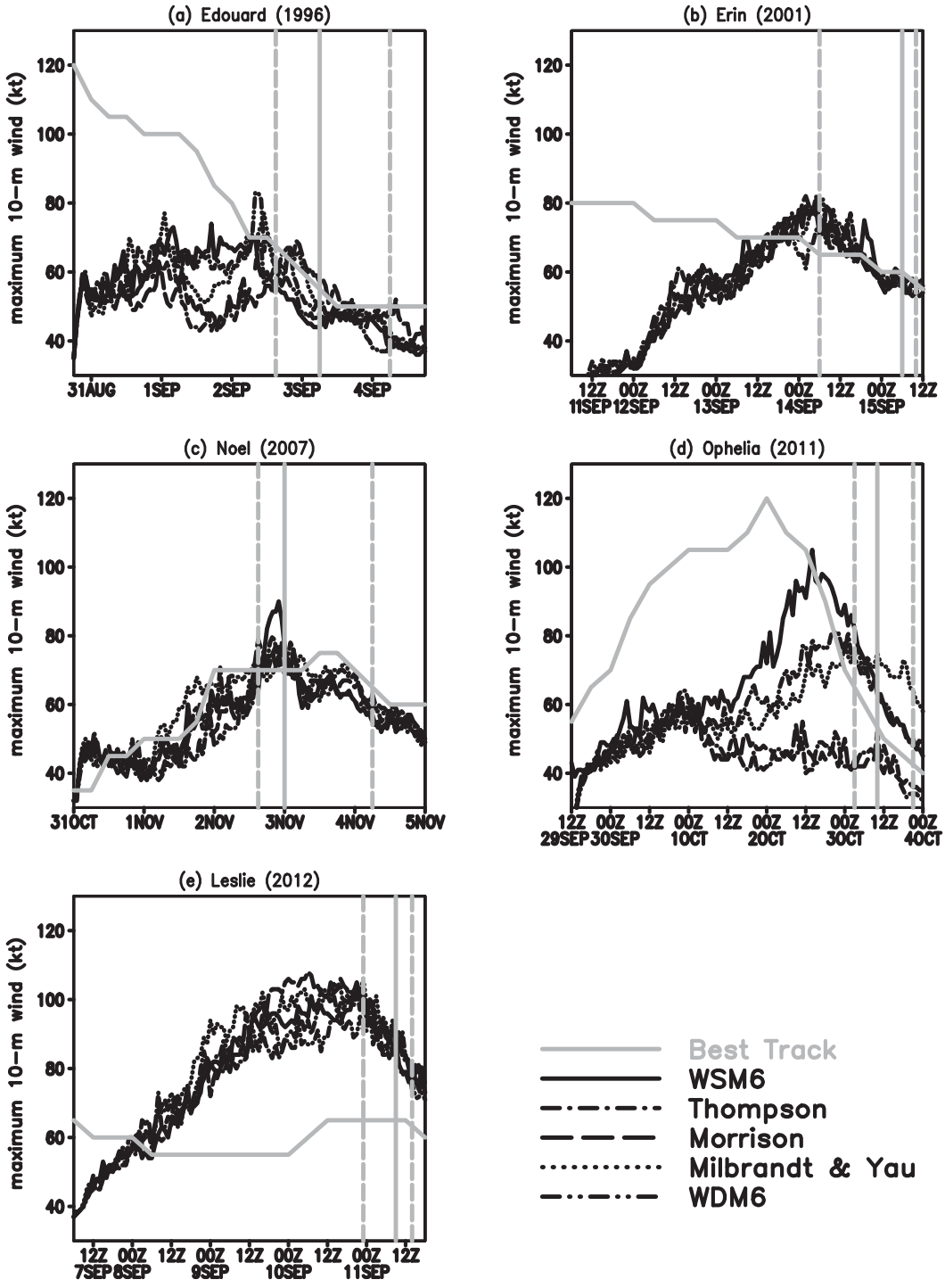

FIG. 3. As in Fig. 2, but for maximum 10-m wind speed v_{max} (kt; where $1\,m\,s^{-1} = 1.94\,kt$).

information related to the simulated TC's structure, latitude, and forward motion in addition to synthetic ADT-derived estimates of v_{max} to obtain estimates of p_{min}. Specifically, the pressure–wind relationship adjusts synthetic ADT-derived estimates of p_{min} away from those derived exclusively from synthetic satellite imagery [derived utilizing DT's tropical pressure–wind relationship for the Atlantic basin, including the latitude bias adjustment of Kossin and Velden (2004)] and toward their corresponding model-simulated values.

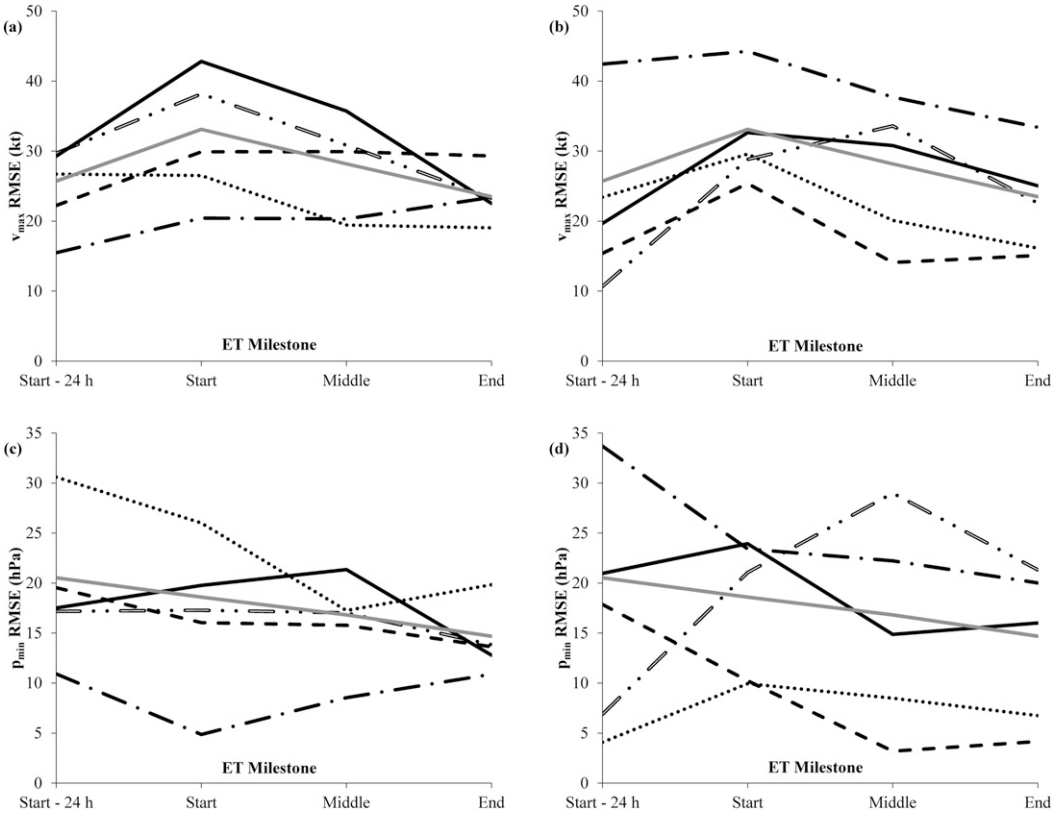

FIG. 4. RMSEs, with respect to the ET timeline of Hart et al. (2006), of (a) v_{max} (kt), as stratified by microphysical parameterization; (b) v_{max} (kt), as stratified by case; (c) p_{min} (hPa), as stratified by microphysical parameterization; and (d) p_{min} (hPa), as stratified by case. The solid gray line in each panel denotes the 23-member composite mean for the variable under consideration. In (a) and (c), the WSM6, Thompson, Morrison, Milbrandt–Yau, and WDM6 composites are represented by solid, dot–dash, dash, dot, and dot–dot–dash lines, respectively. In (b) and (d), the Noel (2007), Leslie (2012), Edouard (1996), Erin (2001), and Ophelia (2011) composites are represented by solid, dot–dash, dash, dot, and dot–dot–dash lines, respectively.

Consequently, RMSE in p_{min} only decreases slightly as synthetic ADT-derived p_{min} estimates and model-simulated p_{min} values evolve in a similar fashion during ET. The bias in synthetic ADT-derived p_{min} estimates is small owing to nearly canceling strong and weak biases stratified by microphysical parameterization, discussed in more detail in section 3b.

b. *Error and bias stratified by case and microphysical parameterization*

The RMSE of v_{max} as stratified by case is depicted in Fig. 4b. To first order, the composite mean RMSE for each of the five cases considered follows a similar evolution to that of the overall composite mean RMSE, generally increasing between $T_B - 24$ h and T_B and decreasing thereafter. The small sample sizes [five simulations for all but Ophelia (2011), for which data from only three simulations are considered] do not permit statistical significance testing for each case, however. At all milestones, particularly at and after T_B, RMSE is directly proportional to the simulated intensity of each case. The case that is, in the composite mean, the most intense during ET, Leslie (2012; Fig. 3e), is associated with the largest RMSE. Conversely, the case that is, in the composite mean, the least intense during ET, Edouard (1996; Fig. 3a), is associated with the smallest RMSE. This is not an unexpected finding: during ET, because the synthetic ADT-derived v_{max} for each case either remains near or rapidly declines toward its minimum-possible value (Fig. 6), cases with higher (lower) model truth v_{max} are associated with larger (smaller) RMSEs. Other distinguishing characteristics, namely time to complete ET and posttransition thermal structure, appear to not be related to RMSE magnitude.

The bias of v_{max} as stratified by case is depicted in Fig. 5b. In most cases, synthetic ADT-derived v_{max} estimates are weak biased. The case that is, in the composite mean, the most intense during ET [Leslie (2012)] is associated with the largest weak bias. However, there is greater case-to-case variability about the overall

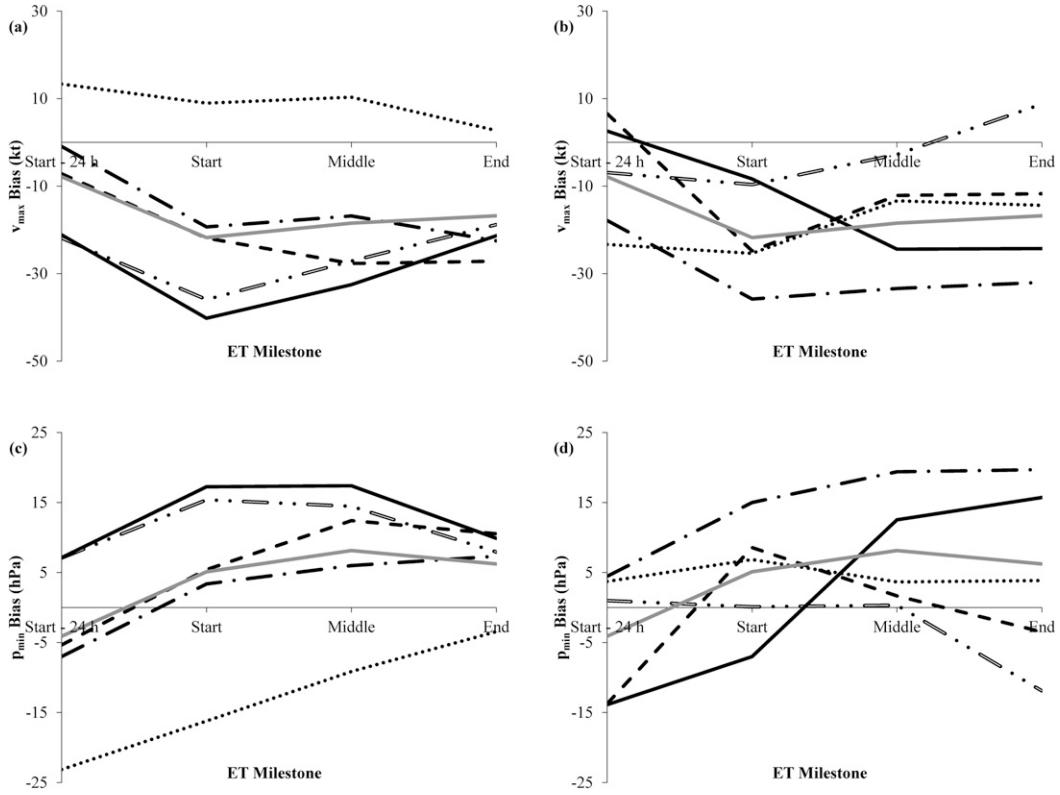

FIG. 5. As in Fig. 4, but for the bias of each field.

composite mean for bias than for RMSE, particularly with respect to Noel (2007) and Ophelia (2011). For each of these cases, small mean biases result from the near cancellation of strong- and weak-biased simulations that stratify by microphysical parameterization. As is discussed in more detail in section 3c, strong-biased simulations generally conducted using the Milbrandt–Yau microphysical parameterization are associated with deeper, more persistent convection during ET compared to their weak-biased counterparts, which are generally conducted using the WSM6 and WDM6 microphysical parameterizations (Figs. 8, 10–13). As ADT-derived intensity estimates heavily rely upon the intensity and organizational extent of deep, moist convection [section 5.H.1 of Olander and Velden (2013)], this results in more intense synthetic ADT-derived v_{max} and, here, strong biases.

The RMSE of p_{min} as stratified by case is depicted in Fig. 4d. To first order, the composite mean RMSE for all cases except Ophelia (2011) becomes smaller throughout ET, similar to the corresponding overall composite mean RMSE. The RMSE of p_{min} is directly proportional to the composite mean simulated intensity of each of the non-Ophelia (2011) cases, particularly at and after T_B (cf. Figs. 2 and 4d). To wit, the composite mean RMSE of p_{min} is larger for Leslie (2012) and Noel (2007) and smaller for Edouard (1996) and Erin (2001). Conversely, the composite mean RMSE for Ophelia (2011) is small at $T_B - 24$ h and grows increasingly large through T_{MID} before decreasing slightly by T_E. This occurs as synthetic ADT-derived estimates of p_{min} increasingly depart from their model-simulated counterparts in the WSM6- and Milbrandt–Yau-based simulations of this case (cf. Figs. 2d and 9d).

The bias of p_{min} as stratified by case is depicted in Fig. 5d. To large extent, the cases that are, in the composite mean, the weakest during ET [Edouard (1996) and Erin (2001)] are associated with the smallest bias magnitudes. An exception occurs with Edouard (1996) at $T_B - 24$ h, in which the case composite mean exhibits a large strong bias. This occurs because the synthetic ADT-derived estimates of p_{min} at this time remain influenced by the National Hurricane Center best-track intensity used to initialize ADT at 1200 UTC 31 August 1996 (Fig. 9a). For Leslie (2012) and Noel (2007), composite mean weak bias grows increasingly large during ET as initially strong-biased simulations—Milbrandt–Yau for Leslie (2012), Milbrandt–Yau and Morrison for Noel (2007)—become weak biased during ET (cf. Figs. 2c,e and 9c,e) as deep, moist convection weakens and is displaced away from the center of

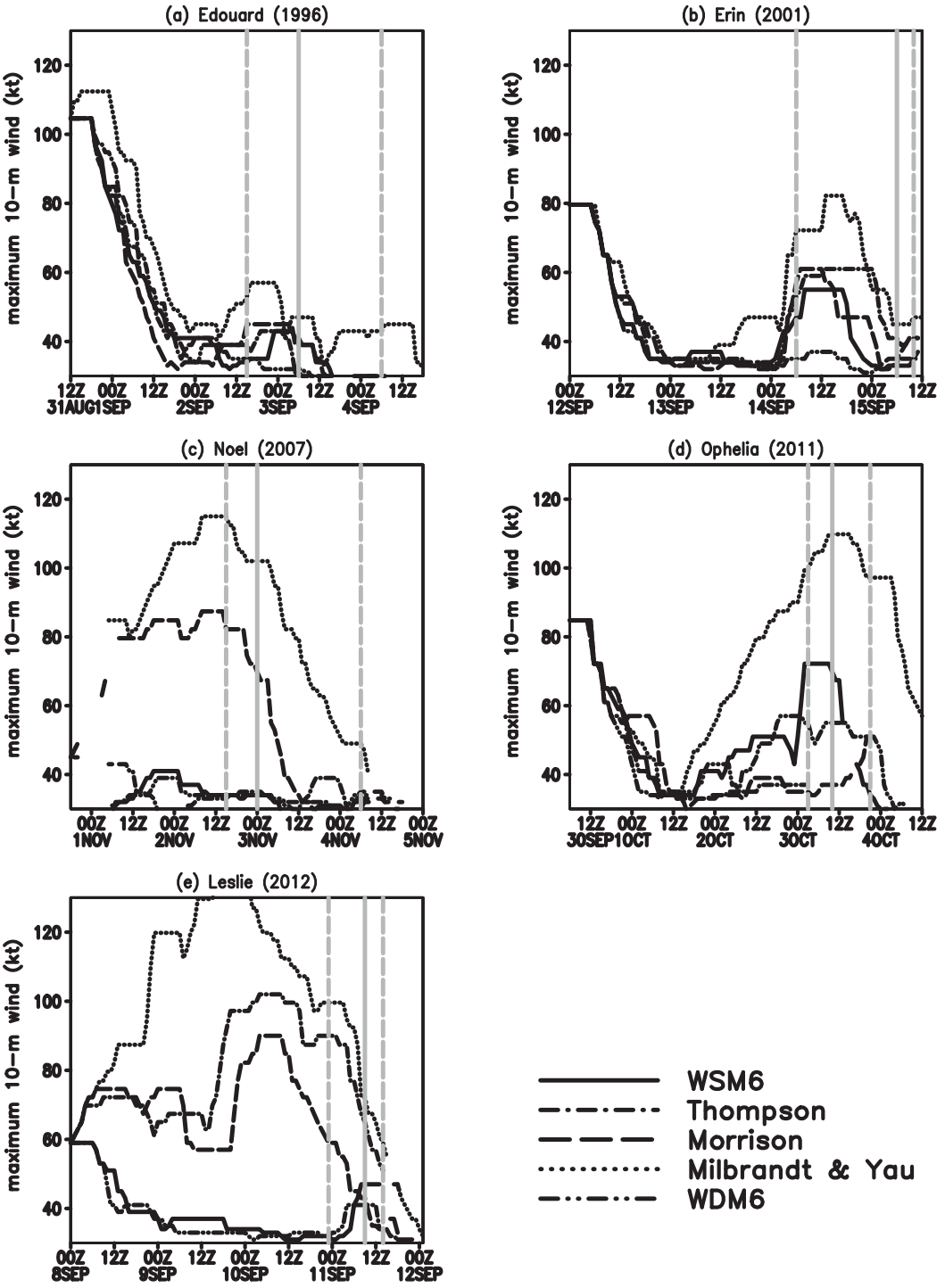

FIG. 6. Synthetic ADT estimates of maximum 10-m wind speed v_{max} (kt) from the WSM6- (solid black), Thompson- (dash–dot), Morrison- (long dash), Milbrandt–Yau- (dot), and WDM6- (dash–dot–dot) based simulations for (a) Edouard (1996), (b) Erin (2001), (c) Noel (2007), (d) Ophelia (2011), and (e) Leslie (2012). The left and right vertical gray dashed lines in each panel reflect the model consensus T_B and T_E, while the vertical gray solid line in each panel reflects the National Hurricane Center–designated T_E. Missing data indicate times at which ADT analyzed the TC to be over land.

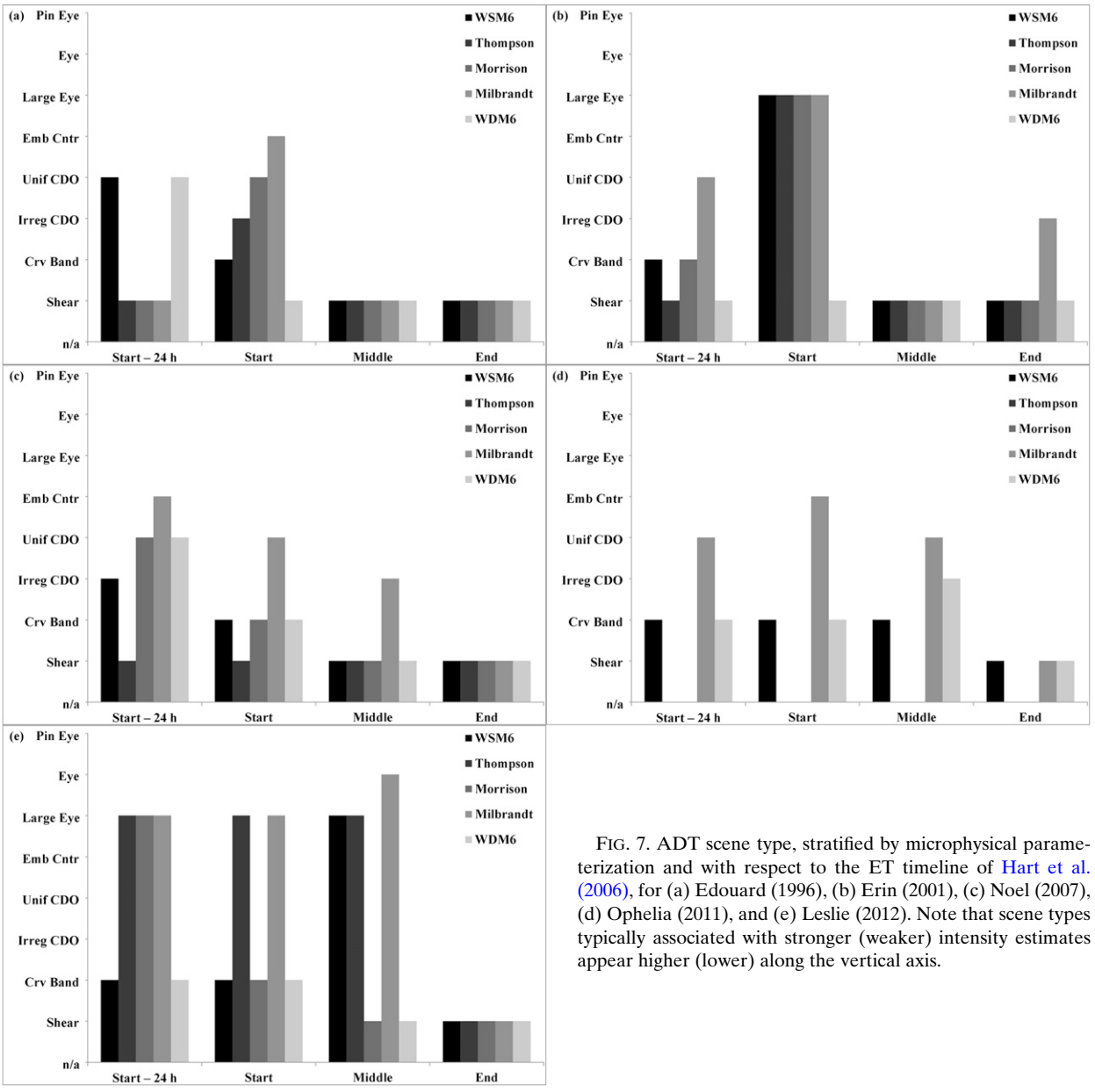

FIG. 7. ADT scene type, stratified by microphysical parameterization and with respect to the ET timeline of Hart et al. (2006), for (a) Edouard (1996), (b) Erin (2001), (c) Noel (2007), (d) Ophelia (2011), and (e) Leslie (2012). Note that scene types typically associated with stronger (weaker) intensity estimates appear higher (lower) along the vertical axis.

the simulated cyclone (Figs. 8 and 10). For Ophelia (2011), the composite mean strong bias grows increasingly large by T_E as the Milbrandt–Yau-based simulation remains strong biased while the bias in the initially weak-biased WSM6- and WDM6-based simulations decreases as the simulated TC rapidly weakens (cf. Figs. 2d and 9d).

The RMSE of $v_{\max}$ as stratified by microphysical parameterization is depicted in Fig. 4a. To first order, the composite mean RMSE for each of the five parameterizations considered follows a similar evolution to that of the overall composite mean RMSE, increasing between $T_B - 24$ h and T_B and declining or remaining approximately constant thereafter. As with the stratification by case, however, the small sample sizes (five simulations for all but Thompson and Morrison, for data from only four simulations are considered) do not permit statistical significance testing on these results. Before T_{MID}, the WSM6- and WDM6-based simulations have the largest composite mean RMSE while the Thompson-based simulations have the smallest composite mean RMSE. By T_E, however, the Morrison-based simulations have the largest composite mean RMSE while the Milbrandt–Yau-based simulations have the smallest composite mean RMSE. With the

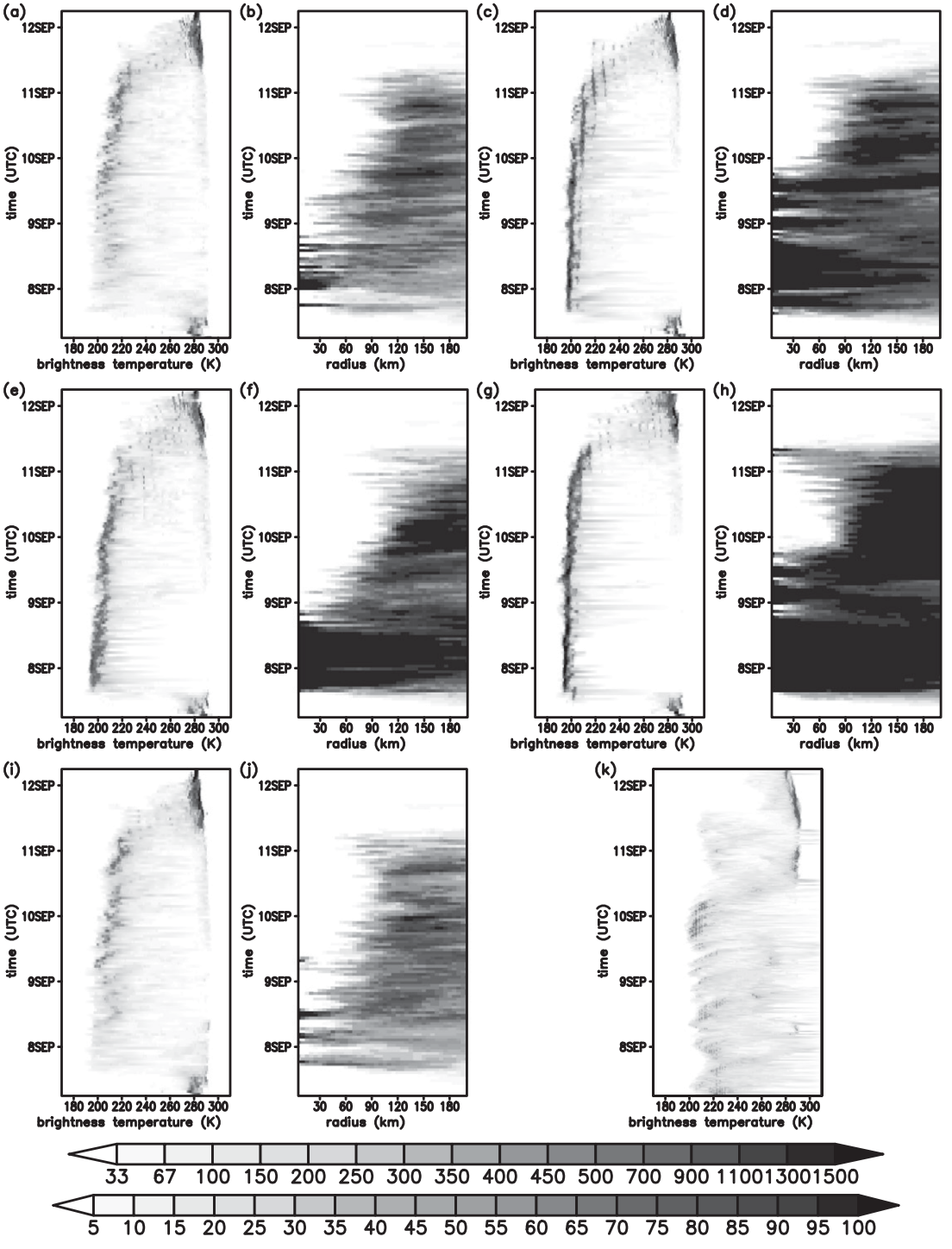

FIG. 8. Hovmöller diagrams of the number of model grid points within ±200 km of the objectively defined cyclone center that contains a given simulated longwave infrared brightness temperature (K; shaded per the topmost color bar), as stratified within 1-K bins between 170 and 310 K, for the (a) WSM6-, (c) Thompson-, (e) Morrison-, (g) Milbrandt–Yau-, and (i) WDM6-based numerical simulations of Leslie (2012). (k) As in (a),(c),(e),(g),(i), but as derived from GOES-East imager channel 4 (10.7 μm) data bilinearly interpolated onto a horizontal grid with $\Delta x = \Delta y = 4$ km. Also displayed are Hovmöller diagrams of the percentage of pixels within 5-km radial bins (%; shaded per the bottommost color bar), out to 200-km radius from the objectively defined cyclone center, with simulated longwave infrared brightness temperature <223 K for the (b) WSM6-, (d) Thompson-, (f) Morrison-, (h) Milbrandt–Yau-, and (j) WDM6-based numerical simulations of Leslie (2012).

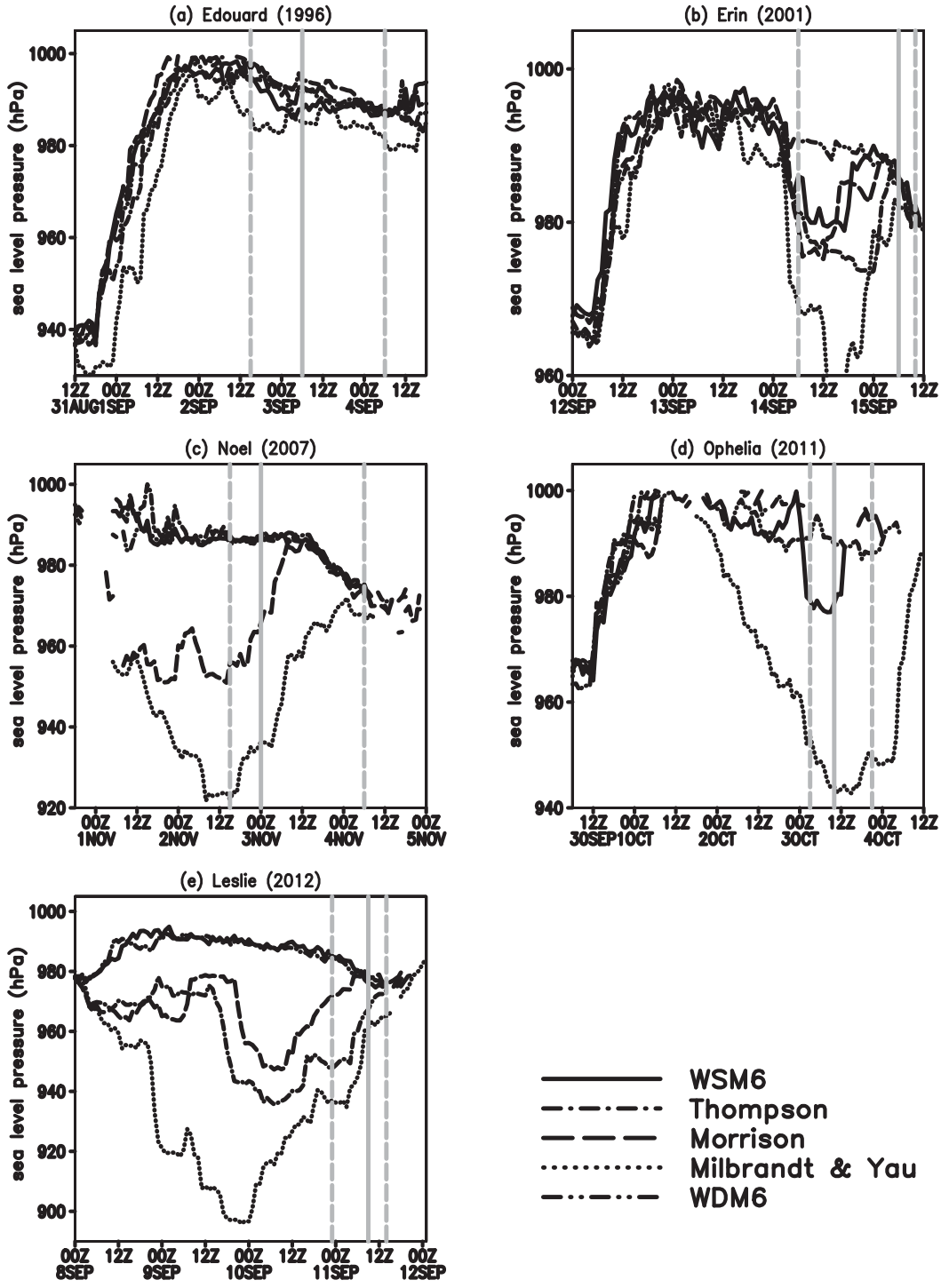

FIG. 9. As in Fig. 6, but for minimum sea level pressure p_{min} (hPa).

exception of the Milbrandt–Yau-based simulations, all are weak biased and evolve in a similar fashion to RMSE (Fig. 5a). By contrast, the Milbrandt–Yau-based composite mean is strong biased prior to T_E and has a near-zero mean bias at T_E.

The RMSE of p_{min} as stratified by microphysical parameterization is depicted in Fig. 4c. The composite mean RMSE for each of the five parameterizations considered resembles that of the overall composite mean. The Thompson-based simulations exhibit the smallest mean

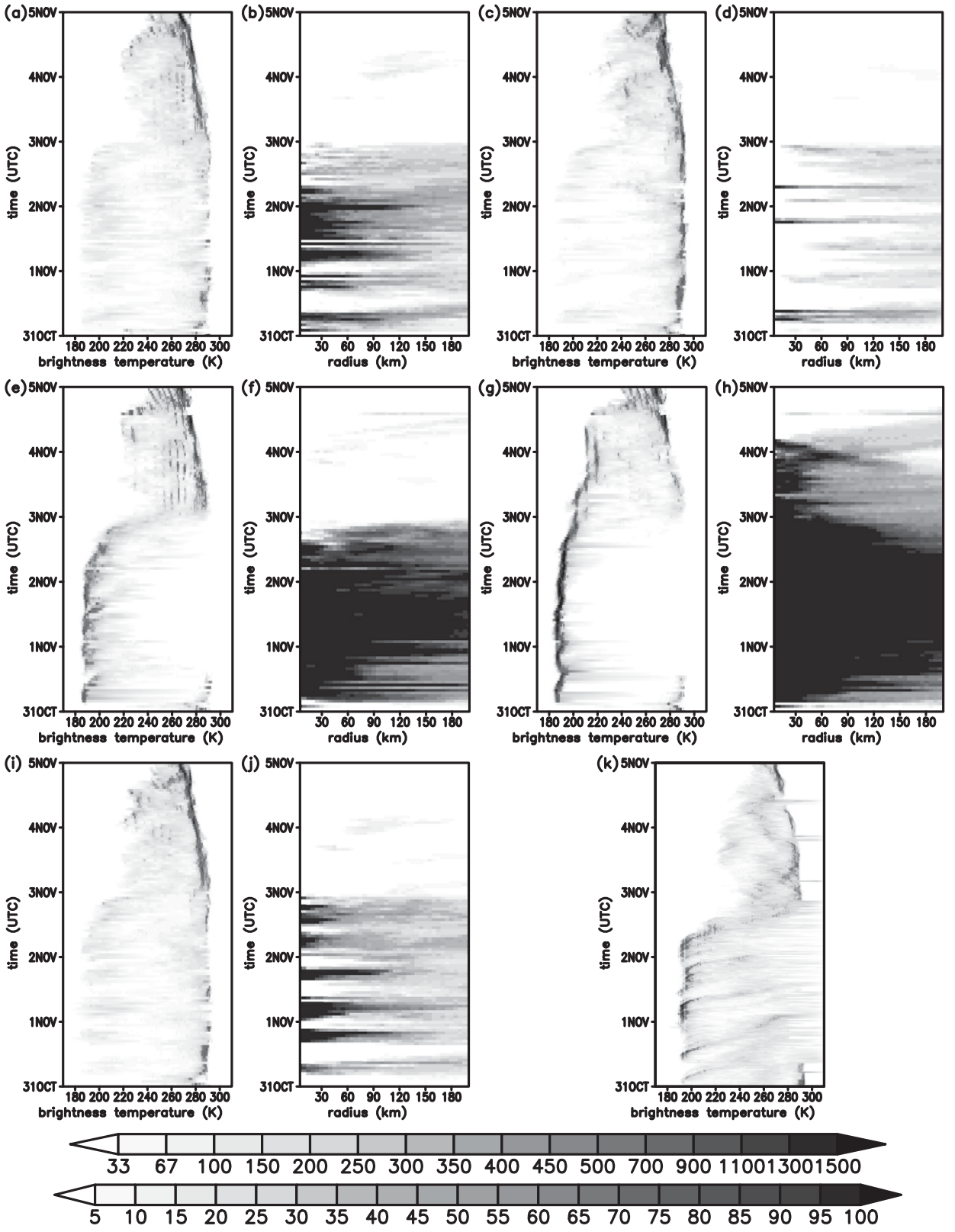

FIG. 10. As in Fig. 8, but for Noel (2007).

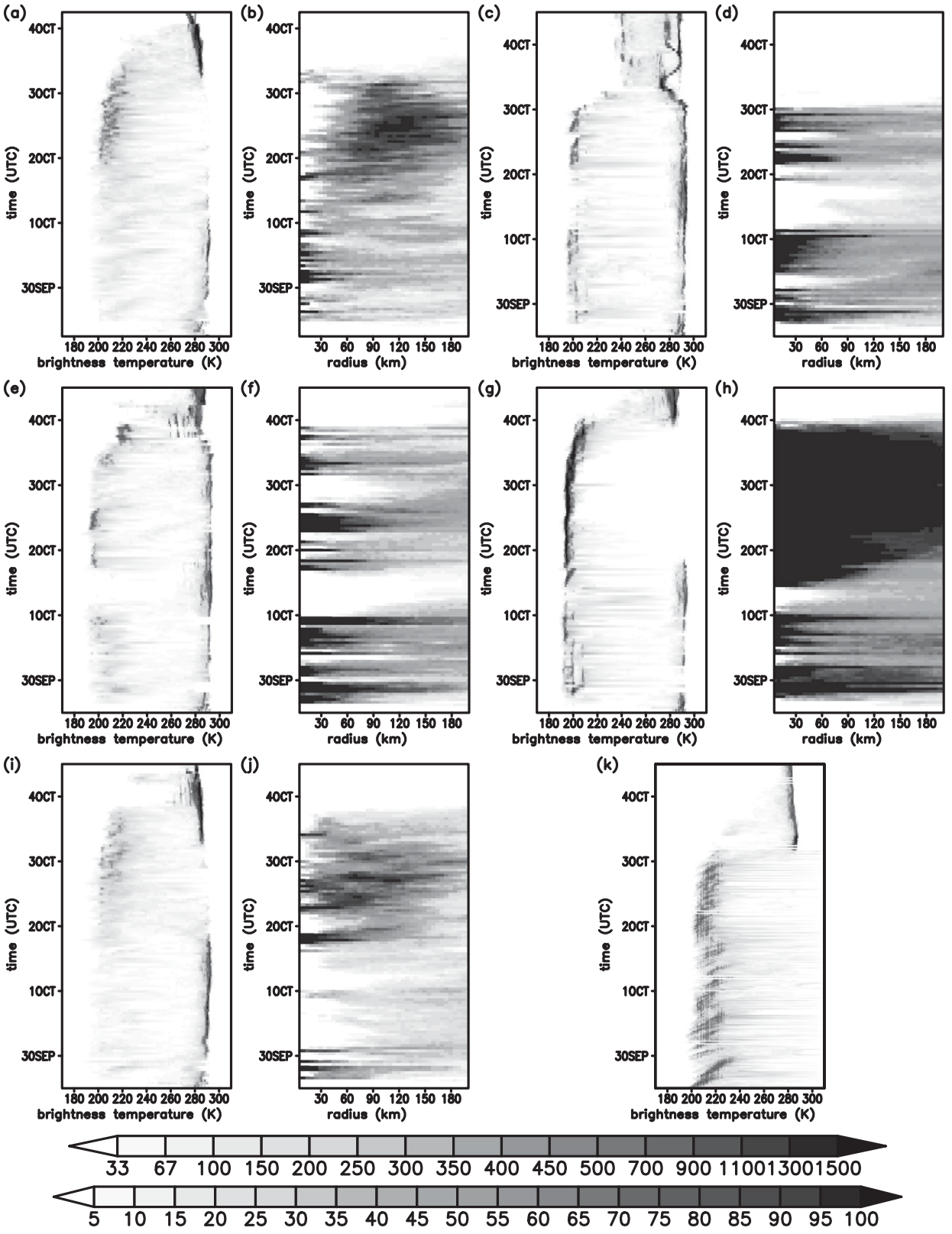

FIG. 11. As in Fig. 8, but for Ophelia (2011).

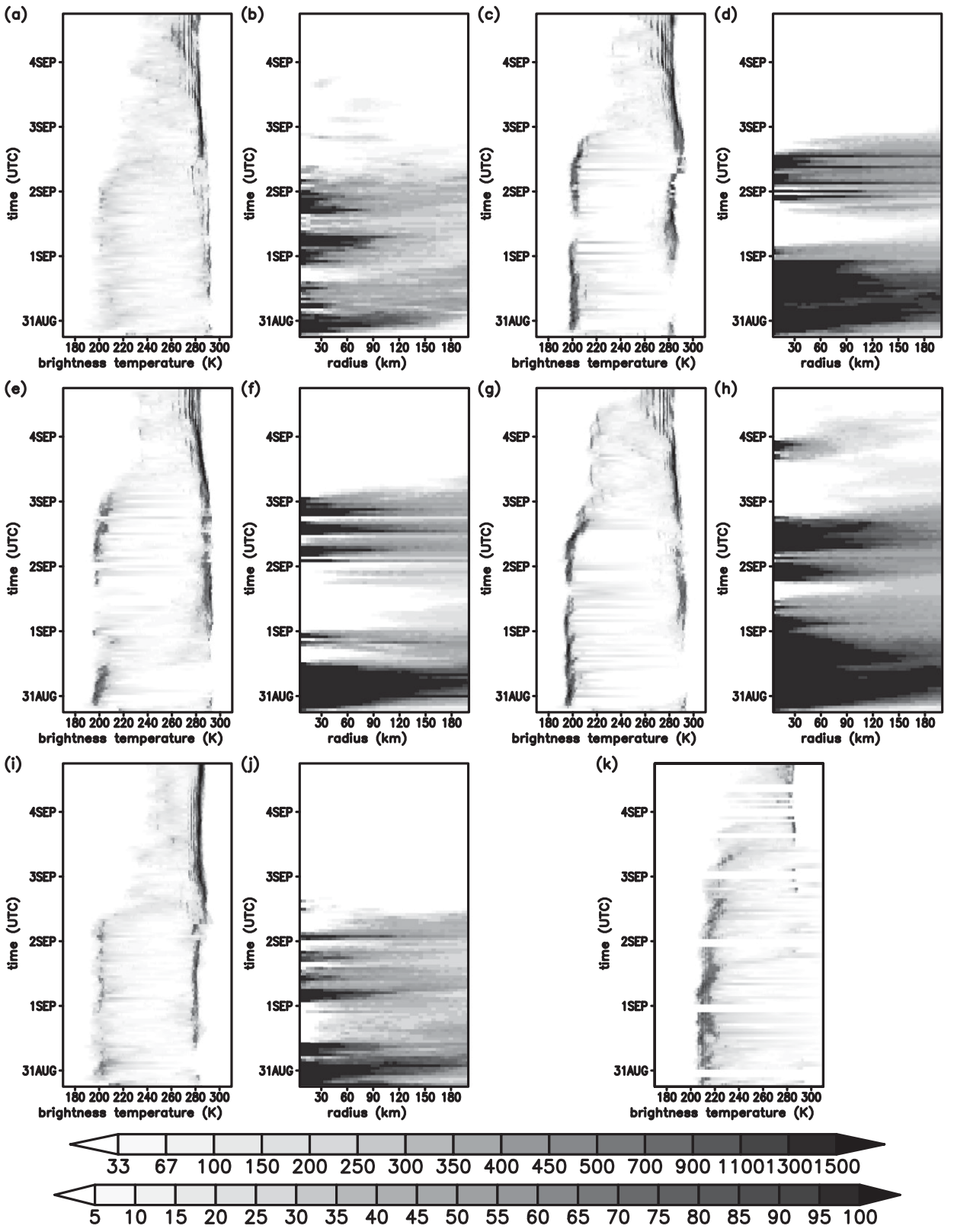

FIG. 12. As in Fig. 8, but for Edouard (1996).

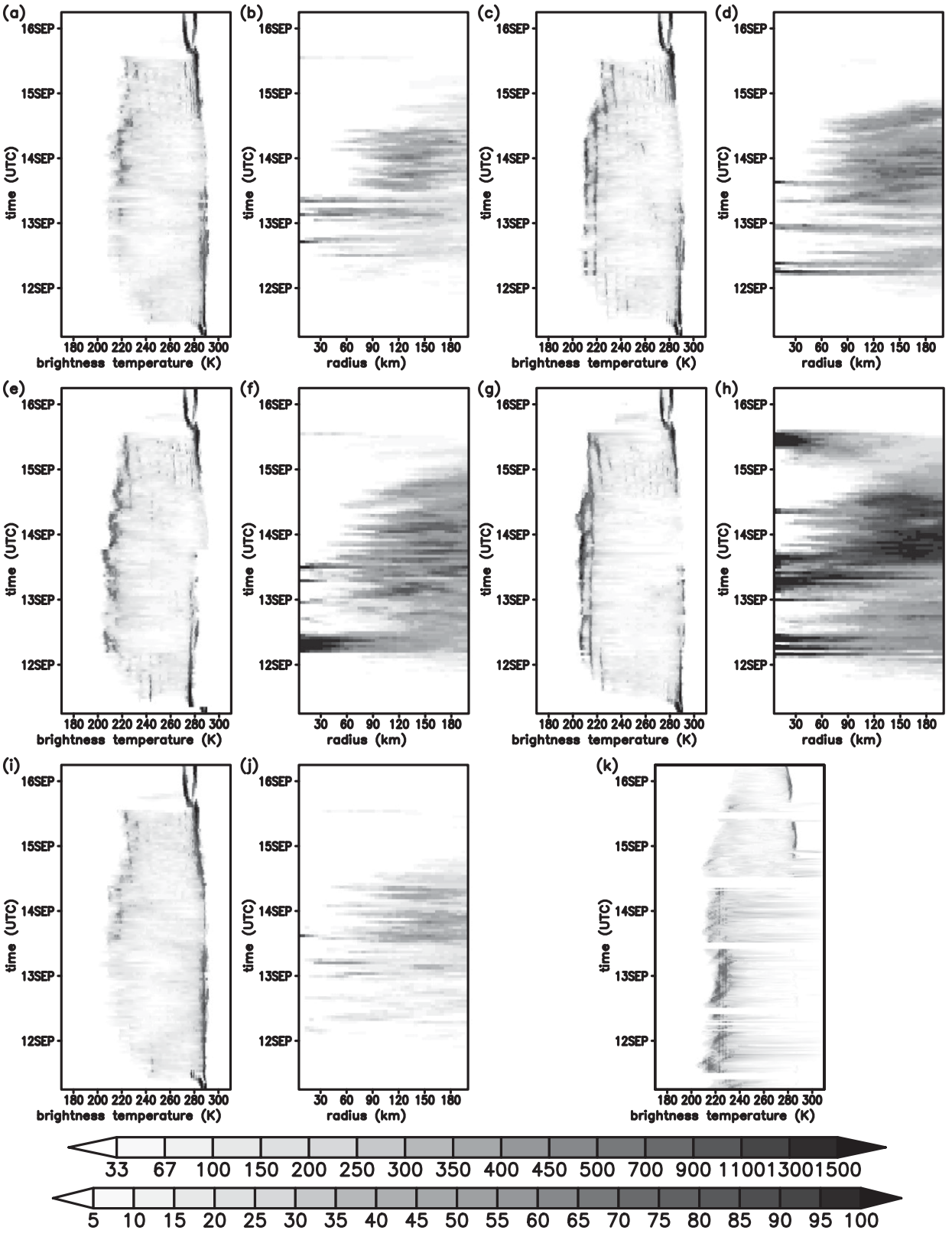

FIG. 13. As in Fig. 8, but for Erin (2001).

RMSEs at all milestones whereas the Milbrandt–Yau-based simulations exhibit the largest mean RMSEs at all milestones except for T_{MID}. The bias of p_{min} as stratified by microphysical parameterization is depicted in Fig. 5c. Overall, the composite mean bias for each parameterization considered resembles that of the overall composite mean. The Milbrandt–Yau-based simulations exhibit a strong bias that decreases in magnitude through ET. The WSM6- and WDM6-based simulations exhibit a comparatively large weak bias at all milestones. The Thompson-based simulations exhibit the smallest bias magnitude at and after T_B.

c. *Interpretation of results*

The Milbrandt–Yau-based simulations are associated with relatively low RMSE for v_{max}, relatively large RMSE for p_{min}, and strong biases for both v_{max} and p_{min}. Brightness temperatures derived from these simulations are colder, and the spatial extent of deep, moist convection is greater, than those both from other simulations and from observations (Figs. 8 and 10–13). This is illustrated by one selected example, from Noel (2007) at T_B, as depicted in Fig. 14, noting that the intensity of each simulated cyclone is approximately equal between simulations (Figs. 2c and 3c). Analysis of area-averaged (within 200 km of the objectively identified TC center) mass mixing ratio fields from each simulation indicates that the Milbrandt–Yau-based simulations of this (Fig. 15) and other cases have greater cloud ice concentrations at greater altitudes. Both factors lead to colder simulated brightness temperatures over a greater area in the Milbrandt–Yau-based simulations, consistent with Cintineo et al. (2014). Consequently, ADT often inferred scene types associated with stronger intensity estimates in the Milbrandt–Yau-based simulations (Fig. 7), resulting in stronger synthetic intensity estimates for these simulations (Figs. 6 and 9, dotted lines). The degree to which these intensity estimates are strong biased is greater for p_{min} than for v_{max}, thus resulting in a comparatively large (small) RMSE for p_{min} (v_{max}).

Conversely, the WSM6- and WDM6-based simulations are generally associated with the greatest RMSE in v_{max} and the largest weak biases for both v_{max} and p_{min}. Brightness temperatures derived from these simulations are warmer, and the spatial extents of the coldest brightness temperatures are smaller, than those from other simulations and from observations (Figs. 8 and 10–13). This is consistent with previous studies that demonstrated a warm bias in brightness temperature and a low bias in convective cloud extent in simulations conducted with the WSM6 microphysical parameterization as compared to observations, whether for tropical (Van Weverberg et al. 2013) or continental (Grasso et al. 2014) mesoscale convective systems. Similar findings are noted for WDM6 in continental convective environments by Cintineo et al. (2014). Both studies attribute this to a deficiency in the amount of simulated upper-tropospheric cloud ice, particularly as compared to other microphysical parameterizations, and the same is true in the simulations presented herein (e.g., Fig. 15). Because synthetic ADT-derived scene type [section 5.B of Olander and Velden (2013)] and intensity estimates [section 5.H.1 of Olander and Velden (2013)] are directly proportional to convective cloud intensity, warmer brightness temperatures result in weaker synthetic ADT-derived intensity estimates for the WSM6- and WDM6-based simulations (Figs. 6 and 9). This can, for instance, result in ADT inferring a noneye scene with weaker inferred intensity when, subjectively, an eye appears to be present. A representative example of this is presented in Fig. 16 for Leslie (2012) at T_B, when ADT inferred a "large eye" scene type for the Thompson- and Milbrandt–Yau-based simulations but a curved-band scene type for the remaining simulations (Fig. 7e). This occurs despite the actual simulated intensity of each cyclone varying minimally between simulations at this time (Figs. 2e and 3e).

It is worth noting that most eye-type scenes inferred by ADT when applied to synthetic satellite imagery are of large-eye type rather than "eye" or "pinhole eye" (Fig. 7). Figure 16 provides a representative example of this for Leslie (2012). This is attributed primarily to the relatively coarse effective resolution of the ARW numerical simulations [~7 Δx, or ~28 km; Skamarock (2004)] rather than to any specific attributes of the selected cases. Further investigation is necessary, however, to conclusively determine the extent to which this may influence the analysis. It should also be noted that most microphysical parameterization–related differences in brightness temperature, and thus simulated cloud properties, for each case occur prior to T_{MID}, with little differences seen as ET completes (as can be inferred from Figs. 8 and 10–13). However, both synthetic ADT-derived scene types and intensity estimates, particularly the current intensity value, rely in part upon their values up to 12 h previous, as constrained by rule 9 (the weakening flag) of Dvorak (1984). Consequently, the influence of differences in simulated cloud properties through T_{MID} upon both RMSE and bias is felt, albeit to progressively smaller extent, through T_E.

4. Summary and discussion

In this study, the utility of synthetic satellite imagery derived from numerical simulations of five ET events that occurred over the open waters of the northern Atlantic Ocean is evaluated to provide insight regarding ADT-derived intensity estimates during ET. Key findings include the following points:

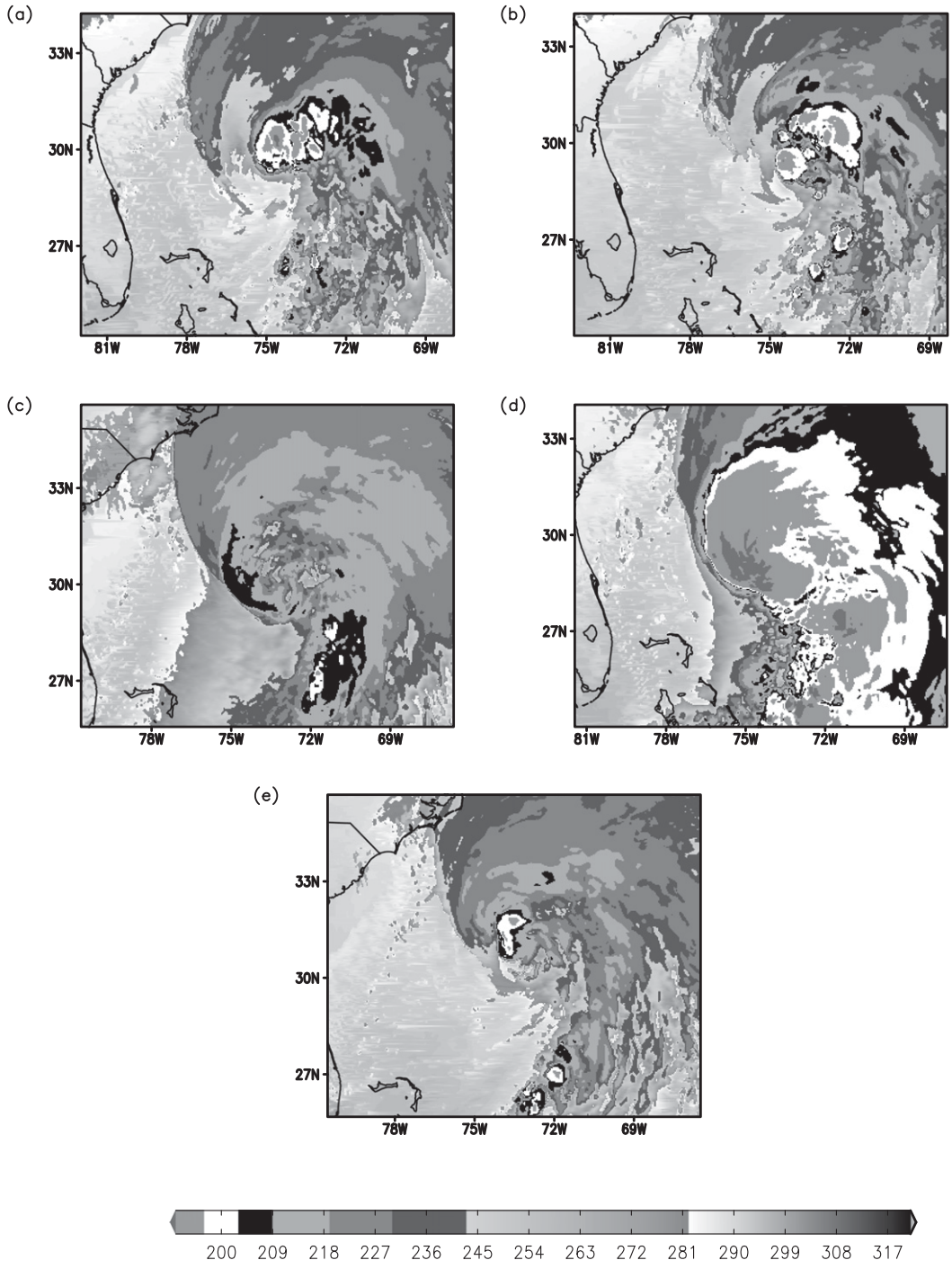

FIG. 14. Simulated longwave infrared brightness temperature (K; shaded; scale is the ''BD'' enhancement scale) at T_B for the (a) WSM6- (1300 UTC 2 Nov), (b) Thompson- (1300 UTC 2 Nov), (c) Morrison- (1900 UTC 2 Nov), (d) Milbrandt–Yau- (1400 UTC 2 Nov), and (e) WDM6- (1800 UTC 2 Nov) based simulations of Noel (2007). The objectively determined TC center is located at the center of each panel.

- On average, synthetic ADT-derived estimates of v_{max} asymptote toward or remain near their weakest-possible values after ET begins. However, both observed and model ''truth'' v_{max} do not weaken as rapidly. Thus, in most cases, RMSE and bias in v_{max} both increase between $T_B - 24$ h and T_B but decrease or remain approximately constant thereafter.

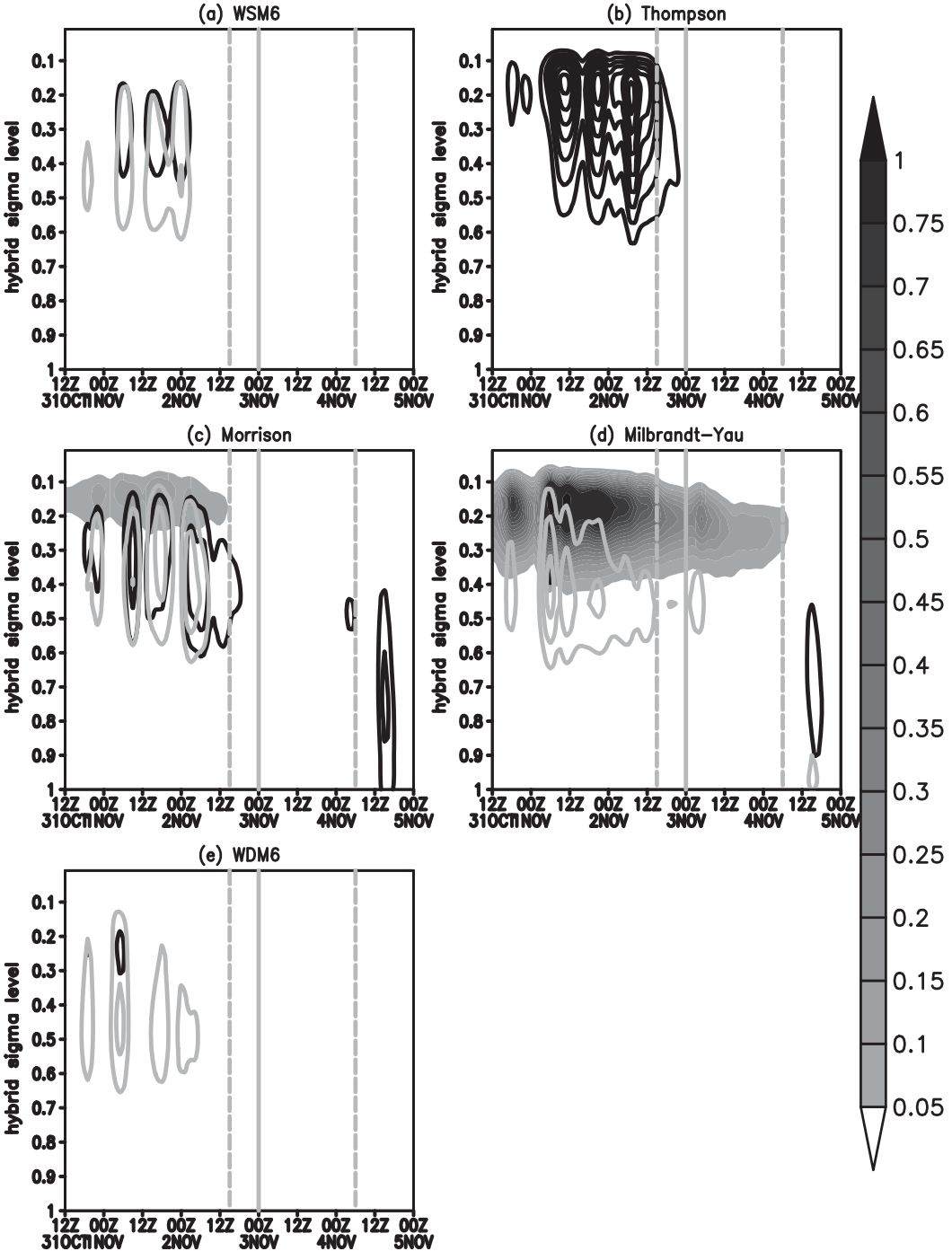

FIG. 15. Area-averaged (within 136 km of the objectively tracked cyclone center) cloud ice mixing ratio q_c (g kg^{-1}; shaded per the color bar at right), snow mixing ratio q_s (g kg^{-1}; black contours every 0.25 g kg^{-1} starting at 0.25 g kg^{-1}), and graupel mixing ratio q_g (g kg^{-1}; gray contours every 0.25 g kg^{-1} starting at 0.25 g kg^{-1}) for numerical simulations of Noel (2007) conducted utilizing the (a) WSM6, (b) Thompson, (c) Morrison, (d) Milbrandt–Yau, and (e) WDM6 microphysical parameterizations between 1200 UTC 31 Oct and 0000 UTC 5 Nov 2007.

- Owing to its incorporation of model-simulated information relating to a simulated TC's structure, latitude, and forward motion, the ADT pressure–wind relationship adjusts synthetic $p_{\min}$ estimates away from those derived exclusively from synthetic satellite imagery toward their corresponding model-simulated values.
- More intense TCs during ET are associated with greater ADT RMSE and bias magnitudes in both $v_{\max}$

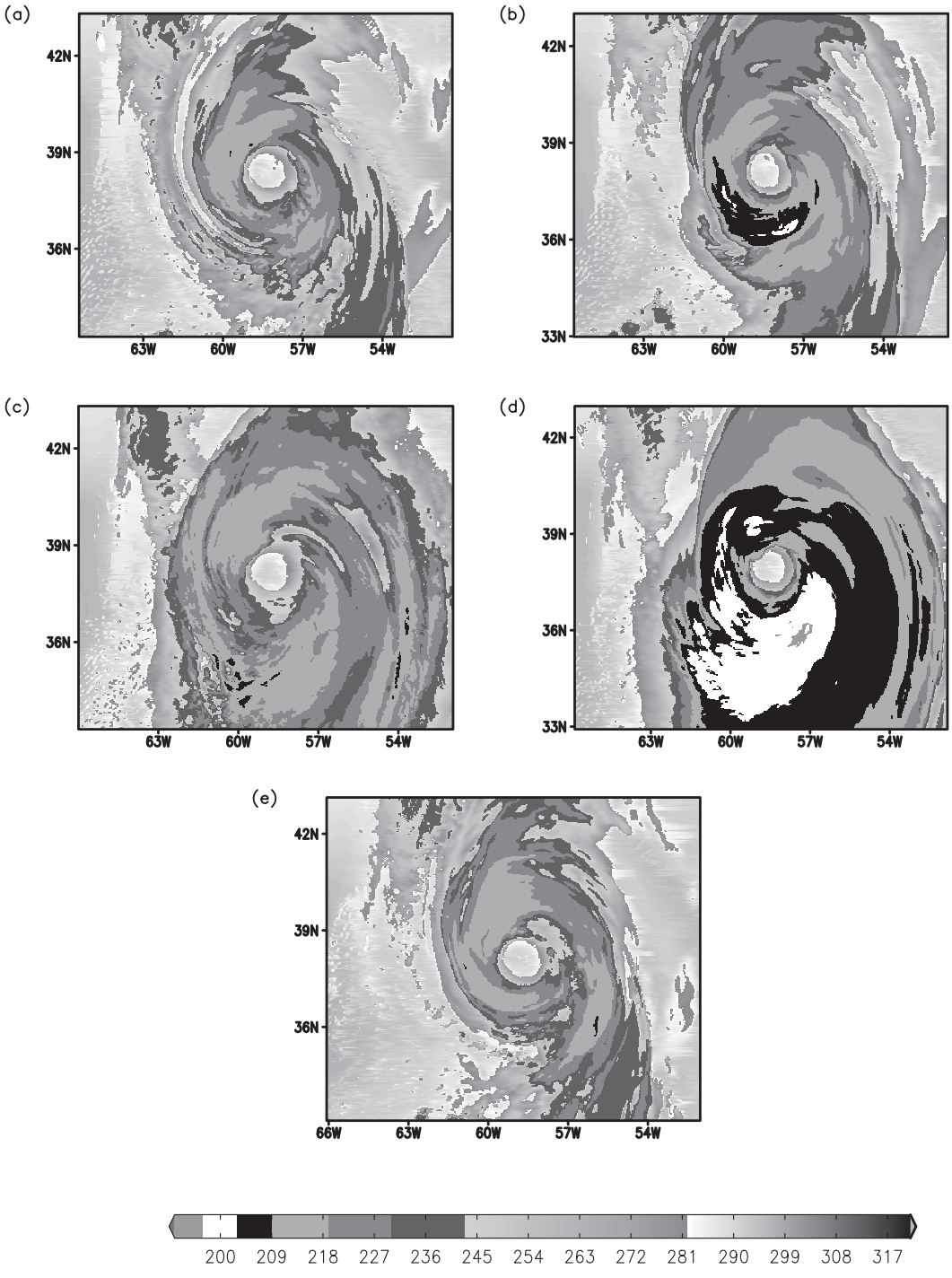

FIG. 16. Simulated longwave infrared brightness temperature (K; shaded, scale is the BD enhancement scale) at T_B for the (a) WSM6- (2200 UTC 10 Sep), (b) Thompson- (2200 UTC 10 Sep), (c) Morrison- (2300 UTC 10 Sep), (d) Milbrandt–Yau- (2300 UTC 10 Sep), and (e) WDM6- (2000 UTC 10 Sep) based simulations of Leslie (2012). The objectively determined TC center is located at the center of each panel.

and p_{min}, although this result does not hold for all cases. Weaker TCs during ET are conversely associated with smaller RMSE and bias magnitudes in both v_{max} and p_{min}.

- Microphysical parameterizations (viz., WSM6 and WDM6) that produce warmer, less expansive upper-tropospheric clouds are associated with weaker synthetic ADT-derived intensity estimates and, consequently,

large RMSE and weak bias for both v_{max} and p_{min}. Conversely, microphysical parameterizations (viz., Milbrandt–Yau) that produce often-unrealistically colder, more expansive upper-tropospheric clouds are associated with stronger synthetic ADT-derived intensity estimates and, as a result, comparatively small RMSE for v_{max}, large RMSE for p_{min}, and strong biases for both v_{max} and p_{min}.

One of the two fundamental questions that this research sought to answer is that of whether reliable ADT-derived intensity estimates for numerically simulated TCs can be obtained by utilizing synthetic satellite imagery derived from numerical simulation output. To that end, the results are decidedly mixed. As the results presented in section 3 demonstrate, RMSE in v_{max} is larger than that of the 18-member observational sample of real (validated) cases motivating our investigation. The bias in v_{max} is larger than that of the observational sample at and after T_B. There are multiple plausible contributors to the discrepancy in both RMSE and bias between the observational and simulated samples. The observational and simulated samples are small and of unequal composition with respect to the cases considered. Because RMSE and bias in v_{max} are functions of the intensity of the transitioning TC for the cases considered herein, samples containing greater numbers of weaker (stronger) TCs will be associated with smaller (larger) RMSE and bias. Furthermore, because RMSE and bias in v_{max} are functions of time during ET, with the smallest values for each found prior to T_B, it is plausible to expect the observational sample, which includes observations up to 48 h prior to T_E, approximately equivalent to $T_B - 24$ h for the five simulated cases, to have smaller RMSE and bias. However, it is not clear that these considerations should result in as large of a discrepancy between the observational and simulated samples as seen herein.

A potentially more problematic contributor lies with the modeling system itself, namely with respect to its ability to accurately simulate cloud radiative properties, as elucidated by synthetic satellite imagery. There is considerable sensitivity in the simulated longwave infrared brightness temperatures to microphysical parameterization that results in considerable variability in the synthetic ADT-derived intensity estimates for both v_{max} (Fig. 6) and p_{min} (Fig. 9). The sensitivity in simulated longwave infrared brightness temperatures to microphysical parameterization results primarily from how cloud ice is treated within each parameterization (e.g., Fig. 15). It should be noted that none of the five microphysical parameterizations utilized herein was developed specifically for tropical applications but rather they were developed for midlatitude and/or continental applications. Given this and the approximate nature of any model parameterization, it is expected that all simulated brightness temperatures are to some extent biased.

Overall, the Thompson and Morrison microphysical parameterization–based numerical simulations produce simulated brightness temperatures that most closely resemble the observations (Figs. 8 and 10–13, cf. panels c and e to k). This is consistent with studies in which the microphysical parameterization's influence upon simulated longwave infrared brightness temperatures was evaluated for both tropical and midlatitude convective phenomena (e.g., Jankov et al. 2011; Van Weverberg et al. 2013; Cintineo et al. 2014; Jin et al. 2014). However, we note that in the composite means for the Thompson- and Morrison-based numerical simulations conducted herein, the RMSE and weak bias in v_{max} remain larger than those for the observational sample. This may be due to differences in sample composition and/or to other factors (e.g., the relatively coarse effective resolution of the numerical model in both the horizontal and vertical directions and its possible impacts upon model output).

However, it should be noted that the sign of the biases in v_{max} is consistent between the observational sample and the numerical simulations. Furthermore, the improvement in synthetic ADT-derived p_{min} estimates fostered by the use of the Knaff and Zehr (rather than Dvorak) pressure–wind relationship is physically well grounded, as described earlier in the manuscript. In light of these considerations, the results suggest that though the application of ADT to synthetic satellite imagery may provide general insight into the evolution of RMSE and bias during ET, it is unable to precisely quantify RMSE or bias for either v_{max} or p_{min} during ET. Consequently, we argue that applying ADT to synthetic satellite imagery obtained from numerical simulations of TCs undergoing ET can be used to gain qualitative, but not quantitative, insight into the nature of the ADT-derived intensity estimate error and bias during ET.

Despite this limitation, the research findings presented herein provide meaningful insight toward how ADT-derived intensity estimates during ET may be improved. Barring substantial improvements in microphysical parameterizations, numerical model simulations are unable to provide accurate quantitative error and bias statistics that may be used to develop a bias correction for ADT applicable during ET. However, if a sufficiently large sample of in situ observations of v_{max} and p_{min} can be obtained, a bias correction method based upon observational data might allow for marginally improved intensity estimates during ET. For such a bias correction method to be feasible, given the results

presented herein, it must be a function of TC intensity, ET milestone, and intensity metric. Of these elements, the first is available a priori whereas the second is not without also incorporating external sources of information (e.g., satellite- or model-derived cyclone-phase information). Furthermore, this bias correction must include a trigger informing ADT whether it should be activated. The erosion of inner-core convection that occurs during ET, as seen in Figs. 8 and 10–13 and as described by Klein et al. (2000), plus information regarding the transitioning TC's position, motion, and current thermal structure (as determined externally), may be utilized to formulate such a trigger. Further research is planned to determine whether sufficient observations exist to develop such a bias correction and to evaluate its performance over an independent sample of events.

Furthermore, it may be possible to develop and subsequently evaluate the performance of an ADT scene type that is specific to ET. As the ''shear'' ADT scene type becomes predominant by the completion of ET, it could be utilized as a starting point for the development of an ET-specific ADT scene type. Incorporating additional information, such as scatterometer estimates of v_{max} when available, reflects one possible modification to this scene type. Alternatively, given that the Miller and Lander (1997) XT and Hebert and Poteat (1975) subtropical cyclone classification and intensity estimation methods closely resemble an empirically modified ''curved band'' ADT scene type, elements of one or both methods could be utilized as a starting point for the development of an ET-specific ADT scene type. Verification of Miller and Lander (1997) and/or Hebert and Poteat (1975) method derived intensity estimates for subtropical and transitioning tropical cyclones may prove insightful with regard to how each might be modified so as to promote improved performance if implemented within an ET-specific ADT scene type. Further research is planned to extend the ADT's capabilities so as to permit subtropical cyclone intensity estimation.

Acknowledgments. Fruitful discussions with Nick Bassill, Jack Beven, Rebecca Cintineo, Derrick Herndon, Sergey Kravtsov, Vince Larson, Dan Lindsey, Jason Otkin, Russ Schumacher, John Sears, and Kyle Swanson were of benefit to this work. Feedback from three anonymous reviewers improved the quality of the content contained within this manuscript. All numerical simulations were conducted on the University of Wisconsin–Milwaukee *avi* supercomputer. We acknowledge the assistance of the University Corporation for Atmospheric Research's *wrfhelp* service with respect to obtaining synthetic satellite imagery from numerical model output.

REFERENCES

Avila, L. A., and S. R. Stewart, 2013: Atlantic hurricane season of 2011. *Mon. Wea. Rev.,* **141,** 2577–2596, doi:10.1175/MWR-D-12-00230.1.

Beven, J. L., 2000: Subtropical storm tropical cyclone report. NHC, 8 pp. [Available online at http://www.nhc.noaa.gov/data/tcr/AL192000_Subtropical.pdf.]

——, S. R. Stewart, M. B. Lawrence, L. A. Avila, J. L. Franklin, and R. J. Pasch, 2003: Atlantic hurricane season of 2001. *Mon. Wea. Rev.,* **131,** 1454–1484, doi:10.1175/1520-0493(2003)131<1454:ASHSO>2.0.CO;2.

Bikos, D., and Coauthors, 2012: Synthetic satellite imagery for real-time high-resolution model evaluation. *Wea. Forecasting,* **27,** 784–795, doi:10.1175/WAF-D-11-00130.1.

Brennan, M. J., R. D. Knabb, M. Mainelli, and T. B. Kimberlain, 2009: Atlantic hurricane season of 2007. *Mon. Wea. Rev.,* **137,** 4061–4088, doi:10.1175/2009MWR2995.1.

Brown, D. B., and J. L. Franklin, 2004: Dvorak TC wind speed biases determined from reconnaissance-based best track data (1997–2003). Preprints, *26th Conf. on Hurricanes and Tropical Meteorology,* Miami, FL, Amer. Meteor. Soc., 3D.5. [Available online at https://ams.confex.com/ams/pdfpapers/75193.pdf.]

Browning, K. A., 1990: Organization of clouds and precipitation in extratropical cyclones. *Extratropical Cyclones: The Erik Palmén Memorial Volume,* C. W. Newton and E. O. Holopainen, Eds., Amer. Meteor. Soc., 129–165.

Carlson, T. N., 1980: Airflow through midlatitude cyclones and the comma cloud pattern. *Mon. Wea. Rev.,* **108,** 1498–1509, doi:10.1175/1520-0493(1980)108<1498:ATMCAT>2.0.CO;2.

Chen, F., and J. Dudhia, 2001: Coupling an advanced land surface–hydrology model with the Penn State–NCAR MM5 modeling system. Part I: Model description and implementation. *Mon. Wea. Rev.,* **129,** 569–585, doi:10.1175/1520-0493(2001)129<0569:CAALSH>2.0.CO;2.

Cintineo, R., J. A. Otkin, M. Xue, and F. Kong, 2014: Evaluating the performance of planetary boundary layer and cloud microphysical parameterization schemes in convection-permitting ensemble forecasts using synthetic *GOES-13* satellite observations. *Mon. Wea. Rev.,* **142,** 163–182, doi:10.1175/MWR-D-13-00143.1.

Courtney, J., and J. A. Knaff, 2009: Adapting the Knaff and Zehr wind-pressure relationship for operational use in tropical cyclone warning centres. *Aust. Meteor. Oceanogr. J.,* **58,** 167–179.

Davis, C., and Coauthors, 2008: Prediction of landfalling hurricanes with the advanced Hurricane WRF model. *Mon. Wea. Rev.,* **136,** 1990–2005, doi:10.1175/2007MWR2085.1.

Dee, D. P., and Coauthors, 2011: The ERA-Interim reanalysis: Configuration and performance of the data assimilation system. *Quart. J. Roy. Meteor. Soc.,* **137,** 553–597, doi:10.1002/qj.828.

Dillon, C. P., and M. J. Andrews, 1998: Joint Typhoon Warning Center 1997 annual tropical cyclone report. JTWC, 216 pp. [Available online at http://www.usno.navy.mil/NOOC/nmfc- ph/RSS/jtwc/atcr/1997atcr.pdf.]

Dvorak, V., 1984: Tropical cyclone intensity analysis using satellite data. NOAA Tech. Rep. NESDIS11, 47 pp. [Available from NOAA/NESDIS, 5200 Auth Rd., Washington, DC 20233.]

Evans, C., and R. E. Hart, 2008: Analysis of the wind field evolution associated with the extratropical transition of Bonnie (1998). *Mon. Wea. Rev.,* **136,** 2047–2065, doi:10.1175/2007MWR2051.1.

Evans, J. L., and R. E. Hart, 2003: Objective indicators of the life cycle evolution of extratropical transition for Atlantic tropical cyclones. *Mon. Wea. Rev.,* **131,** 909–925, doi:10.1175/1520-0493(2003)131<0909:OIOTLC>2.0.CO;2.

Garratt, J. R., 1992: *The Atmospheric Boundary Layer.* Cambridge University Press, 316 pp.

Grasso, L., D. T. Lindsey, K.-S. S. Lim, A. Clark, D. Bikos, and S. R. Dembek, 2014: Evaluation of and suggested improvements to the WSM6 microphysics in WRF-ARW using synthetic and observed *GOES-13* imagery. *Mon. Wea. Rev.,* **142,** 3635–3650, doi:10.1175/MWR-D-14-00005.1.

Han, Y., P. van Delst, Q. Liu, F. Weng, B. Yan, R. Treadon, and J. Derber, 2006: JCSDA Community Radiative Transfer Model (CRTM)—Version 1. NOAA Tech. Rep. NESDIS 122, 40 pp.

Hart, R. E., 2003: A cyclone phase space derived from thermal wind and thermal asymmetry. *Mon. Wea. Rev.,* **131,** 585–616, doi:10.1175/1520-0493(2003)131<0585:ACPSDF>2.0.CO;2.

——, J. L. Evans, and C. Evans, 2006: Synoptic composites of the extratropical transition life cycle of North Atlantic tropical cyclones: Factors determining posttransition evolution. *Mon. Wea. Rev.,* **134,** 553–578, doi:10.1175/MWR3082.1.

Hebert, P. H., and K. O. Poteat, 1975: A satellite classification technique for subtropical cyclones. NOAA Tech. Memo. NWS SR-83, 25 pp.

Hong, S.-Y., and J.-O. J. Lim, 2006: The WRF single-moment 6-class microphysics scheme (WSM6). *J. Korean Meteor. Soc.,* **42,** 129–151.

——, Y. Noh, and J. Dudhia, 2006: A new vertical diffusion package with an explicit treatment of entrainment processes. *Mon. Wea. Rev.,* **134,** 2318–2341, doi:10.1175/MWR3199.1.

Iacono, M. J., J. S. Delamere, E. J. Mlawer, M. W. Shephard, S. A. Clough, and W. D. Collins, 2008: Radiative forcing by long-lived greenhouse gases: Calculations with the AER radiative transfer models. *J. Geophys. Res.,* **113,** D13103, doi:10.1029/2008JD009944.

Jankov, I., and Coauthors, 2011: An evaluation of five ARW-WRF microphysics schemes using synthetic GOES imagery for an atmospheric river event affecting the California coast. *J. Hydrometeor.,* **12,** 618–633, doi:10.1175/2010JHM1282.1.

Jarvinen, B. R., C. J. Neumann, and M. A. S. Davis, 1984: A tropical cyclone data tape for the North Atlantic basin, 1886–1983: Contents, limitations, and uses. NOAA Tech. Memo. NWS NHC-22, Coral Gables, FL, 21 pp.

Jimenez, P. A., J. Dudhia, J. F. Gonzalez-Rouco, J. Navarro, J. P. Montavez, and E. Garcia-Bustamante, 2012: A revised scheme for the WRF surface layer formulation. *Mon. Wea. Rev.,* **140,** 898–918, doi:10.1175/MWR-D-11-00056.1.

Jin, Y., and Coauthors, 2014: The impact of ice phase cloud parameterizations on tropical cyclone prediction. *Mon. Wea. Rev.,* **142,** 606–625, doi:10.1175/MWR-D-13-00058.1.

Jones, S. C., and Coauthors, 2003: The extratropical transition of tropical cyclones: Forecast challenges, current understanding, and future directions. *Wea. Forecasting,* **18,** 1052–1092, doi:10.1175/1520-0434(2003)018<1052:TETOTC>2.0.CO;2.

Klein, P. M., P. A. Harr, and R. L. Elsberry, 2000: Extratropical transition of western North Pacific tropical cyclones: An overview and conceptual model of the transformation stage. *Wea. Forecasting,* **15,** 373–395, doi:10.1175/1520-0434(2000)015<0373:ETOWNP>2.0.CO;2.

Knaff, J. A., and R. M. Zehr, 2007: Reexamination of tropical cyclone wind–pressure relationships. *Wea. Forecasting,* **22,** 71–88, doi:10.1175/WAF965.1.

Kossin, J. P., and C. S. Velden, 2004: A pronounced bias in tropical cyclone minimum sea level pressure estimation based on the Dvorak technique. *Mon. Wea. Rev.,* **132,** 165–173, doi:10.1175/1520-0493(2004)132<0165:APBITC>2.0.CO;2.

Landsea, C. W., and J. L. Franklin, 2013: Atlantic hurricane database uncertainty and presentation of a new database format. *Mon. Wea. Rev.,* **141,** 3576–3592, doi:10.1175/MWR-D-12-00254.1.

Lim, K.-S. S., and S.-Y. Hong, 2010: Development of an effective double-moment cloud microphysics scheme with prognostic cloud condensation nuclei (CCN) for weather and climate models. *Mon. Wea. Rev.,* **138,** 1587–1612, doi:10.1175/2009MWR2968.1.

Milbrandt, J. A., and M. K. Yau, 2005: A multimoment bulk microphysics parameterization. Part II: A proposed three-moment closure and scheme description. *J. Atmos. Sci.,* **62,** 3065–3081, doi:10.1175/JAS3535.1.

Miller, D. W., and M. A. Lander, 1997: Intensity estimation of tropical cyclones during extratropical transition. JTWC Rep. JTWC/SATOPS/TN-97/002, 9 pp.

Morrison, H., G. Thompson, and V. Tatarskii, 2009: Impact of cloud microphysics on the development of trailing stratiform precipitation in a simulated squall line: Comparison of one- and two-moment schemes. *Mon. Wea. Rev.,* **137,** 991–1007, doi:10.1175/2008MWR2556.1.

Olander, T. L., and C. S. Velden, 2007: The advanced Dvorak technique: Continued development of an objective scheme to estimate tropical cyclone intensity using geostationary infrared satellite imagery. *Wea. Forecasting,* **22,** 287–298, doi:10.1175/WAF975.1.

——, and ——, 2013: ADT—Advanced Dvorak technique users' guide (McIDAS version 8.1.4). Cooperative Institute for Meteorological Satellite Studies and Space Science and Engineering Center, University of Wisconsin–Madison, 70 pp. [Available online at http://tropic.ssec.wisc.edu/misc/adt/guides/ADTV8.1.4_Guide.pdf.]

Otkin, J. A., and T. J. Greenwald, 2008: Comparison of WRF model-simulated and MODIS- derived cloud data. *Mon. Wea. Rev.,* **136,** 1957–1970, doi:10.1175/2007MWR2293.1.

——, ——, J. Sieglaff, and H.-L. Huang, 2009: Validation of a large-scale simulated brightness temperature dataset using SEVIRI satellite observations. *J. Appl. Meteor. Climatol.,* **48,** 1613–1626, doi:10.1175/2009JAMC2142.1.

Pasch, R. J., and L. A. Avila, 1999: Atlantic hurricane season of 1996. *Mon. Wea. Rev.,* **127,** 581–610, doi:10.1175/1520-0493(1999)127<0581:AHSO>2.0.CO;2.

Seemann, S. W., E. E. Borbas, R. O. Knuteson, G. R. Stephenson, and H.-L. Huang, 2008: Development of a global infrared land surface emissivity database for application to clear sky sounding retrievals from multispectral satellite radiance measurements. *J. Appl. Meteor. Climatol.,* **47,** 108–123, doi:10.1175/2007JAMC1590.1.

Skamarock, W. C., 2004: Evaluating mesoscale NWP models utilizing kinetic energy spectra. *Mon. Wea. Rev.,* **132,** 3019–3032, doi:10.1175/MWR2830.1.

——, and Coauthors, 2008: A description of the advanced Research WRF version 3. NCAR Tech. Note NCAR/TN–475+STR, 125 pp. [Available online at http://www2.mmm.ucar.edu/wrf/users/docs/arw_v3.pdf.]

Stewart, S. R., 2013: Tropical cyclone report: Hurricane Leslie (AL122012). NHC, 19 pp. [Available online at http://www.nhc.noaa.gov/data/tcr/AL122012_Leslie.pdf.]

Thompson, G., P. R. Field, R. M. Rasmussen, and W. D. Hall, 2008: Explicit forecasts of winter precipitation using an improved bulk microphysics scheme. Part II: Implementation of a new snow parameterization. *Mon. Wea. Rev.,* **136,** 5095–5115, doi:10.1175/2008MWR2387.1.

Van Weverberg, K., and Coauthors, 2013: The role of cloud microphysics parameterization in the simulation of mesoscale convective system clouds and precipitation in the tropical western Pacific. *J. Atmos. Sci.,* **70,** 1104–1128, doi:10.1175/JAS-D-12-0104.1.

Velden, C., and Coauthors, 2006: The Dvorak tropical cyclone intensity estimation technique: A satellite-based method that has endured for over 30 years. *Bull. Amer. Meteor. Soc.,* **87,** 1195–1210, doi:10.1175/BAMS-87-9-1195.

Zhu, T., and D.-L. Zhang, 2006: Numerical simulation of Hurricane Bonnie (1998). Part II: Sensitivity to varying cloud microphysical processes. *J. Atmos. Sci.,* **63,** 109–127, doi:10.1175/JAS3599.1.